Local comparisons of tropospheric ozone: Vertical soundings at two neighbouring stations in Southern Bavaria

Thomas Trickl[1], Martin Adelwart[2], Dina Khordakova[3], Ludwig Ries[4], Christian Rolf[3],
Michael Sprenger[5], Wolfgang Steinbrecht[2] and Hannes Vogelmann[1]

[1]Karlsruher Institut für Technologie, Institut für Meteorologie und Klimaforschung (IMK-IFU), Kreuzeck-bahnstr. 19, D-82467 Garmisch-Partenkirchen, Germany

[2]Deutscher Wetterdienst, Meteorologisches Observatorium, Albin-Schwaiger-Weg 10, 82383 Hohenpeißenberg, Germany

[3]Forschungszentrum Jülich, IEK-7, Wilhelm-Johnen-Straße, 52425 Jülich, Germany

[4]Umweltbundesamt II 4.5, Plattform Zugspitze, GAW-Globalobservatorium Zugspitze-Hohenpeißenberg, Schneefernerhaus, 82475 Zugspitze, Germany

[5]Eidgenössische Technische Hochschule (ETH) Zürich, Institut für Atmosphäre und Klima, Universitätstraße 16, 8092 Zürich, Switzerland

Correspondence to: Dr. Thomas Trickl, thomas@trickl.de, Thomas-Knorr-Str. 47, D-82467 Garmisch-Partenkirchen, Germany; tel. +49-8821-50283; Dr. Hannes Vogelmann, hannes.vogelmann@kit.edu, Karlsruher Institut für Technologie, IMK-IFU, Kreuzeckbahnstr. 19, D-82467 Garmisch-Partenkirchen, Germany; tel: +49-8821-258

Abstract. In this study ozone profiles of the differential-absorption lidar Garmisch-Partenkirchen are compared with those of ozone sondes of the Forschungszentrum Jülich and of the Meteorological Observatory Hohenpeißenberg (German Weather Service). The lidar measurements are quality assured by the highly accurate *in-situ* measurements at nearby the Wank (1780 m a.s.l.) and Zugspitze (2962 m a.s.l.) summits and at the Global Atmosphere Watch station Schneefernerhaus (2670 m a.s.l.). The lidar results agree almost perfectly with those of the monitoring stations. Side-by-side sounding of the lidar and electrochemical (ECC) sonde measurements by a team of the Forschungszentrum Jülich shows just small positive offsets (≤ 3.4 ppb), almost constant within the troposphere. We conclude that the recently published uncertainties of the lidar in the final configuration since 2012 are realistic and rather small for low to moderate ozone. Comparisons with the Hohenpeißenberg routine Brewer-Mast sonde measurements are more demanding because of the distance of 38 km between both sites. These comparisons cover the three years September 2000 to August 2001, 2009 and 2018. A slight negative average offset (−3.64 ppb ± 7.5 ppb (full error)) of the sondes with respect to the lidar is found. Most sonde measurements could be improved in the troposphere by recalibration with the station data. This would not only remove the average offset, but also greatly reduce the variability of the individual offsets. The comparison for 2009 suggests a careful partial re-evaluation of the lidar measurements between 2007 and 2011 for altitudes above 6 km where an occasional negative bias occurred.

Key words: Tropospheric ozone, ozone sonde, lidar, differential absorption

1. Introduction

The development of tropospheric ozone has been studied over more than a century (e.g., Gaudel et al., 2018; Tarasick et al., 2019). For many decades, balloon-borne ozone sondes have been a primary work horse of ozone profiling. Their measurement principle is based on the oxidation of iodide (I⁻) to iodine (I_2) by ozone in a wet-chemical potassium iodide (KI) cell. Between cathode and anode of the wet-chemical cell, the oxidation reaction drives an electrical current which can be measured (two electrons per ozone molecule). Recently, nearly all

Atmospheric
Measurement
Techniques
Open Access

Discussions

EGU

41 stations have used the so-called ECC (electro-chemical-cell) sonde type (Komhyr 1969; 1995), featuring two

42 cells with different potassium iodide concentrations (anode and cathode cell). Only the Hohenpeißenberg station,

43 discussed here, still uses the older-type Brewer-Mast sondes (Brewer and Milford, 1960), which uses one cell

44 only (with a platinum cathode and a silver anode), and a less efficient pump design (Steinbrecht et al., 1998).

45 Ozone sondes have been characterized in numerous studies, both in flight (e.g., Attmannspacher and Dütsch,

46 1981; De Muer and Malcorps, 1984; Beekmann et al., 1994; Kerr et al., 1994; Jeannet et al., 2007; in recent

47 years: Gaudel et al., 2015; Van Malderen et al., 2016; Deshler et al., 2017; Tarasick et al., 2021; Ancellet et al.,

48 2022; Stauffer et al., 2022), and in a laboratory simulation chamber (Smit et al., 2007, 2014, 2021). Generally,

49 the accuracy of individual ECC soundings for ozone in the mid-latitude troposphere is about 5 to 10% (Logan et

50 al., 2012; Smit et al., 2014; Tarasick et al., 2016, 2019). Following rigorous best practices, 5% accuracy can be

51 achieved (Vömel et al., 2020; Smit et al., 2021; Tarasick et al., 2021). For Brewer-Mast soundings, the accuracy

52 is slightly lower in the troposphere, about 10 to 15% (Smit et al. 2014; Tarasick et al., 2016, 2019).

53 The ozone soundings at the Meteorological Observatory Hohenpeißenberg (MOHp) of the German Weather

54 Service (Deutscher Wetterdienst, DWD) in Southern Bavaria have been routinely carried out since November

55 1966, yielding one of the longest ozone-sonde time series. Brewer-Mast ozone sonde data tend to have a low

56 bias above about 25 km altitude (Steinbrecht et al., 1998). In the troposphere, compared to ECC soundings,

57 Tarasick et al. (2002, 2016) [?] negative bias of about 20 % for ozone from Canadian Brewer-Mast soundings

58 prior to 1980. European Brewer-Mast stations, however, have generally used a much more extensive preparation

59 procedure for their sondes (Claude et al. 1987), and no significant tropospheric bias has been reported for their

60 routine Brewer-Mast soundings (de Backer et al. 1998; Stübi et al. 2008; Logan et al., 2012), as well as in

61 chamber experiments (Smit et al., 2014).

62 Routine measurements with ozone sondes yield time series free of a fair-weather bias. However, the balloon

63 ascents take place at intervals of several days. Ozone profiles at short intervals can be provided by lidar

64 sounding, but are limited to clear atmospheric conditions. Lidar measurements can generate altitude-time curtain

65 plots and, thus, give much better insight into the impact of atmospheric transport (e.g., Browell et al., 1987;

66 Ancellet et al., 1991; Langford et al., 1996).

67 At IFU (Fraunhofer-Institut für Atmosphärische Umweltforschung; now: Karlsruher Institut für Technologie,

68 IMK-IFU) in Garmisch-Partenkirchen (Germany), a differential-absorption lidar (DIAL) with a particularly wide

69 operating range from next to the ground up to the upper troposphere was completed in 1990 in the framework of

70 the TESLAS (Tropospheric Environmental Studies by Laser Sounding) subproject of EUROTRAC (TESLAS,

71 1997; EUROTRAC, 1997, Kempfer et al., 1994). Subsequently, the system was applied for a full year (1991)

72 within the TOR (Tropospheric Ozone Research; Kley et al., 1997) subproject of EUROTRAC (Carnuth et al.,

73 2002). The operating range of this system was extended upwards to roughly 15 km in 1994 by introducing three-

74 wavelength operation (Eisele et al., 1999).

75 Until 2003 the system was used for individual research projects. Between 2007 and 2018 routine measurements

76 took place, parallel to lidar measurements of water vapour (Vogelmann and Trickl, 2008) and aerosol. The

77 complementary information from these instruments has made possible a large number of investigations related to

78 atmospheric transport. The IFU ozone DIAL was recently fully described by Trickl et al. (2020a).

79 The distance between MOHp and IFU is just 38 km which offers a good chance for comparisons. Due to its

80 design, the IFU ozone DIAL features particularly low uncertainties. However, such a comparison must be made

81 with care since the atmospheric variability is high on a rather small scale (Vogelmann et al., 2011; 2015), mostly

82 caused by the advection of air masses from rather different source region and altitudes, with different

Atmospheric
Measurement
Techniques
Discussions

83 concentrations (e.g., Stohl and Trickl, 1999; Trickl et al., 2003; Trickl et al., 2011). The variability of the vertical

84 distribution of ozone measurements rarely yields very strong concentration changes, but the concentration

85 changes are extreme for water vapour (Vogelmann et al., 2011; 2015). Our lidar measurements of water vapour

86 exhibit a concentration span of more than two decades, with minima of the relative humidity (RH) clearly below

87 1 % in layers descending from the stratosphere (Trickl et al., 2014; 2015; 2016; Klanner et al., 2021).

88 Comparisons between the MOHp sonde and the IFU lidar were made in the second half of the 1990s and in

89 2001, after the first upgrading of the lidar A few of these comparisons in 1996 and 1997 were published by

90 Eisele et al. (1997; 1999). For the six cases with sufficient air-mass matching a principal agreement in the middle

91 and upper troposphere to within 5 ppb prevailed with occasional departures of the order of 10 ppb.

92 Hints on ozone differences between the Zugspitze (2962 m a.s.l..) *in-situ* data and the MOHp values (H. E.

93 Scheel, personal communication around 2010) for 3 km a.s.l. have led to a revived interest in a thorough

94 comparison. There have been speculations about an influence of a different air composition outside the

95 mountains at low altitudes up to a few kilometres.

96 In this paper we first characterize the lidar performance by side-by-side ascents of ozone-sondes by a team of the

97 Forschungszentrum Jülich (FZJ). Then, we give a statistical assessment for the measurements at IFU and MOHp

98 for 2018. For this year we achieved the best coverage of by DIAL measurements. This allows us to make an air-

99 mass related data selection to improve the comparison. After the shutdown of the IFU stations in 2012,

100 comparisons have been made exclusively with the Global Atmosphere Watch (GAW) routine *in-situ*

101 measurements at the Schneefernerhaus high-altitude station (UFS, 2671 m a.s.l.). UFS is located just below the

102 Zugspitze summit. Finally, we also compare lidar and MOHp sonde for two earlier development phases of the

103 lidar, for which ozone reference data at the local summit stations Wank (1780 m a.s.l.) and Zugspitze exist.

104 **2. Methods**

105 **2.1 Brewer-Mast sonde system at Hohenpeißenberg**

106 MOHp is located on an isolated mountain outside the Alps, 38 km to the north of IMK-IFU and 50 km to the

107 south-west of Munich (975 m a.s.l., 47.80 N, 11.00 E). Brewer-Mast ozone sondes have been launched on a

108 regular basis since November 1966. The sondes undergo a rigorous preparation procedure (Claude et al. 1987),

109 which has remained essentially unchanged since the early 1970s. From 1995 to 2005, Vaisala RS80 radiosondes

110 and a Vaisala PC-CORA ground station have been used in combination with the ozone sondes. This was

111 changed to Vaisala RS92 radiosondes and DigiCora III MW31 ground equipment in 2005, to MW41 ground

112 station in 2018, and to Vaisala RS41 radiosondes in 2019. The standard processing does not subtract a

113 background current, but ozone sondes with non-negligible background current on the ground (> 2.5 ppb ozone)

114 are not flown. Pump temperature is assumed to be constant at 300 K, which compensates to some degree for a

115 too weak pump correction in the stratosphere (Steinbrecht et al. 1998). A time-lag correction is not applied, but

116 this is not critical outside regions with steep ozone gradients. Each ozone profile is adjusted by multiplication

117 with an altitude-independent correction factor, so that the total ozone column estimated from the sounding

118 (including an extrapolation above approximately 30 km) matches the more accurate total ozone measurement

119 from on-site Dobson or Brewer spectrometers, or from satellite instruments. This so-called "Dobson correction"

120 generally improves that accuracy of the ozone sounding data in the stratosphere, but may introduce a small bias

121 in the tropospheric data of some soundings (e.g., Stübi et al., 2008; Logan et al. 2012).

122 The MOHp ozone sonde and radiosonde data are stored in the data base of the Network for the Detection of

123 Atmospheric composition change (NDACC), from where they were imported for the study presented here.

Atmospheric
Measurement
Techniques
Discussions

Open Access

EGU

124 **2.2 ECC sonde system of the Forschungszentrum Jülich (FZJ)**

125 A mobile ballon-borne sonde system of FZJ was operated at IMK-IFU (at 730 m a.s.l.), in close vicinity to the

126 ozone DIAL, during the FIRMOS measurement campaign (Klanner et al., 2020; Palchetti et al., 2021; Di Natale,

127 2021). Several balloons with cryogenic frostpoint hygrometers (CFH; Vömel et al., 2007; 2016), standard

128 Vaisala RS-41-SGP radiosondes (Vaisala et al., 2019), En-Sci ECC ozone sondes (Komhyr et al., 1995; Smit et

129 al., 2007) and COBALD backscatter sondes (Brabec, 2011) were launched. The data were transmitted to a

130 ground station installed for this campaign at the Zugspitze summit. The combined balloon payload is well tested

131 and regularly also used by the GCOS Reference Upper Air Network (GRUAN) (e.g., Dirksen et al., 2014).

132 We followed the standard operating procedures (SOP) of Smit et al. (2014) for the sonde preparation using a

133 solution composition of 1 % and 1/10 (one-tenth) buffer for best results with sondes from the manufacturer En-

134 Sci (Thompson et al., 2019).

135 For the analysis of the ECC data, the methods described by Vömel et al. (2020) are used, i.e., time lag correction

136 and background current correction. The overall uncertainty of the ozone measurements of the ECC sondes is 5%.

137 Due to the obstruction of the line of sight between between launch site at IMK-IFU and the ground station at the

138 summit by the Waxenstein mountain allowed data recording only from approximately 1500 m altitude upwards.

139 Therefore, we used the estimated ECC background current from the sonde preparation one day before a flight as

140 starting value for the background correction instead of the actual measured profile from ground up to 1500 m.

141 This results in an additional uncertainty in the lower part of the profile (2 to 3 km a.s.l.).

142 **2.4 IFU ozone DIAL system**

143 The ozone DIAL of IMK-IFU (Garmisch-Partenkirchen), located at 47.477 N, 11.064 E, and 740 m a.s.l., has

144 been developed and optimized since 1988 (Kempfer et al., 1994; Trickl et al., 2020a). It is based on a krypton

145 fluoride excimer laser, operated at 400 mJ per pulse (40 W) of narrowband radiation at 248.5 nm, two

146 Newtonian receiving telescopes (diameter of the primary mirrors: 0.13 m and 0.5 m) and 1.1-m grating

147 spectrographs for wavelength separation. Efficient stimulated Raman shifting in hydrogen and deuterium yields

148 emission at the three operating wavelengths 277.2 nm, 291.8 nm and 313.2 nm. The shorter-wave spectral

149 components are absorbed by ozone ("on" wavelengths), that at 313.2 nm ("off" or reference wavelength) is

150 almost outside the absorption region of O_3. The laser system is operated with a repetition rate of 99 Hz which

151 allows a short data-acquisition time of just 41 s.

152 The shortwave 277.2-nm emission yields particularly accurate measurements, but the strong extinction of this

153 radiation by ozone limits the range to about 8 km. The performance in the two 277.2-nm channels is robust with

154 respect to minor misalignment, with uncertainties of about 2 to 3 ppb. This is not the case for 291.8 nm where

155 the optical alignment must be controlled with care because of less tight focussing into the entrance slit of the far-

156 field spectrograph. In addition, the 291.2-nm backscatter signal is three times noisier than that for 277.2-nm. The

157 noise of the 313.2-nm signal becomes important at large distances. As a consequence, the uncertainty of the

158 ozone mixing ratio can be become rather high in the upper troposphere and the tropopause region, in particular in

159 summer due to the stronger loss of signal caused by the higher levels of ozone. Sometimes the uncertainty just

160 below the tropopause can even exceed 10 ppb.

161 The DIAL data processing is made for different wavelength combinations (Eisele and Trickl, 2005). In this way,

162 an internal quality control can be achieved. The optical alignment is optimized immediately after detecting an

163 ozone mismatch in the first quicklook data evaluation. Just the laser beam overlap of the different wavelength

164 components (Trickl et al., 2020a) and the beam pointing must be optimized.

Atmospheric
Measurement
Techniques
Discussions
Open Access

EGU

165 The calibration of the lidar measurements has been based from the very beginning (1991) on the accurate

166 temperature-dependent ozone absorption cross sections of the University of Reims (Daumont et al., 1992;

167 Malicet et al., 1995). These cross sections were verified for four wavelengths below 300 nm by Viallon et al.

168 (2015) to within ±0.06 %. In the presence of aerosol an aerosol correction is made with the algorithms of Eisele

169 and Trickl (2005). This correction is rather robust for the wavelength pair 277 nm - 292 nm because of the strong

170 absorption at the short "on" wavelength and the moderate wavelength difference (Völger et al., 1996).

171 Meteorological data for calculating density and temperature profiles are taken from the Munich radiosonde

172 (station 10868). The retrieved 313-nm aerosol backscatter coefficients have been routinely stored in the data

173 base of the European Aerosol Lidar Network (EARLINET) since 2007.

174 After repeated system upgrading the final performance of the lidar was reached in late 2012. In the absence of

175 aerosol the far-field ozone could be evaluated with high reliability from the 291.0-nm signal alone, after

176 precisely modelling the air number density from radiosonde data. In this way the daytime noise induced by the

177 division by the 313-nm data in summer could frequently be avoided.

178 During the final decade of the lidar operation a fitting procedure was applied in noisy situations in the upper

179 troposphere (i.e., under high-ozone conditions in summer). This procedure reduces unrealistic curvature of ozone

180 structures caused by enhanced data smoothing, and, thus, abrupt concentration changes (in particular at the

181 tropopause) visible in the raw data are reproduced in the mixing ratio. We prepared an extension of the data-

182 acquisition time from 41 s to about five minutes in order to improve the signal-to-noise ratio. However, the lidar

183 operation ended before the start of this option.

184 From 1991 to 2003 the DIAL was operated for focussed research projects. Routine measurements took place

185 from 2007 to 2018, until 2015 parallel to measurements with a water-vapour DIAL (Trickl et al., 2014, 2015,

186 2016, 2020b). In 2012 the highest data quality was finally reached, which included significant improvements for

187 the near-field telescope (Trickl et al., 2020a). Thus, the conditions for a meaningful system validation were

188 obtained. The operation was discontinued in February 2019, after the retirement of the first author of this paper.

189 **2.5 *In-situ* measurements**

190 Quality-assured ozone measurements at Wank (1780 m a.s.l., 7.0 km to the north-east of IMK-IFU, 47.511º

191 N, 11.141º E) and Zugspitze (2962 m a.s.l., 8.4 km to the south-west of IMK-IFU, 47.421º N, 10.986º E) took

192 place from 1978 to 2012. Since the 1990s two or three TE 49 analysers (Thermo Environmental Instruments,

193 USA) were operated simultaneously at each station. These instruments are based on ultraviolet (UV) absorption

194 at 253.65 nm. Several comparisons using transfer standards (O_3 calibrators TE 49 PS) were made with the World

195 Meteorological Organization (WMO) Global Atmosphere Watch (GAW) reference instrument kept at the

196 WMO/GAW calibration centre operated by EMPA, Switzerland (Klausen et al., 2003). The most recent

197 comparison was conducted in June 2006 and confirmed that the Zugspitze O_3 data are on the GAW scale.

198 Apart from the two mountain stations measurements were performed also at IFU at about 740 m a.s.l. (47.477º

199 N, 11.064º E). This laboratory was adjacent to that of the ozone DIAL.

200 At UFS (0.70 km to the south-east of Zugspitze, 47.417º, 10.980º E) ozone has been continuously measured

201 since 2002 by a team of the German Federal Environment Agency (Umweltbundesamt, UBA) using TEI 49i

202 instruments (Thermo Electron Corporation). The gas inlet is at 2671 m a.s.l. As ozone standard for weekly and

203 monthly calibration a TEI 49C-PS instrument was applied that was calibrated against the ozone standard of UBA

204 (UBA SRP#29) on an annual basis. UBA operates the German standard for Ozone. It was adjusted via BIPM

205 (Bureau International des Poids et Mesures) in Paris to the NIST ozone reference standard of the WMO/GAW

Atmospheric
Measurement
Techniques
Discussions

Open Access
EGU

206   measurement programme. The measurements were supported by a second instrument (Horiba APOA-370). The
207   instrumentation is fully adequate for Global Atmosphere Watch monitoring. GAW system and performance
208   audits at the station for surface ozone took place in 2001, 2006 and 2011.

209   The uncertainty of the *in-situ* ozone measurements is ±0.5 ppb with respect to the WMO standard (Hearn et al.,
210   1961). This fulfills the GAW requirement.

211   The ozone data for all sites are stored at half-hour intervals. The times are specified for the end of the averaging
212   interval in Central European Time (CET, = UTC + 1 h). 1-h averages for the Zugspitze stations were made
213   available to the World Data Center and the TOAR data base (Schultz et al., 2017). In the present study we use
214   data at half-hour time resolution.

215   **2.6 LAGRANTO Trajectories**

216   Fifteen-day backward trajectories were calculated with the Lagrangian Analysis tool (LAGRANTO; Sprenger
217   and Wernli, 2015; Wernli and Davies 1997). The driving wind fields are obtained from the ERA5 reanalysis
218   dataset (Hersbach et al., 2020), which we interpolated to a 0.5º latitude/longitude grid, and on 137 vertical hybrid
219   levels. The input ERA5 data are available at a one-hour temporal resolution; the output positions of the
220   trajectories are written at 15-min time interval to allow for a more refined analysis. The starting coordinates of
221   the backward trajectories are 11.064 E, 47.477 N, and the starting altitudes match the altitudes of interest in the
222   soundings (see Sect. 4). The start times of the trajectories correspond to the sounding times within five minutes.
223   Finally, the start times are also shifted by several hours relative to the sounding time to assess the sensitivity of
224   the trajectory calculation on time.

225   **3. Results**

226   The main problem in comparing vertical sounding is illustrated in Fig. 1 which shows several ozone measure-
227   ments at Garmisch-Partenkirchen and Hohenpeißenberg in the morning of 2 October 2017. The vertical
228   distributions during that period are characterized by a descending stratospheric intrusion layer (see low relative
229   humidity) of rapidly diminishing width and significant changes at all altitudes on a short time scale. This reveals
230   the spatially highly inhomogeneous air mass. The approximate agreement of lidar and Hohenpeißenberg ozone
231   sonde before 6:00 CET is, thus, fortuitous. At different altitudes different air components must be assumed as
232   indicated by matching of the sonde ozone with lidar measurements at different times.

233   Until 2010 the lidar results were routinely compared with the long-term measurements at Wank and Zugspitze.
234   Apart from occasional orographically induced deviations an agreement to within ±2 ppb was found. After these
235   *in-situ* measurements were terminated we have routinely compared the lidar measurements with the ozone
236   measurements at UFS. Mostly a similar agreement is found.

237   **3.1 Comparisons of the IFU ozone lidar and the Jülich ECC sonde**

238   An optimum lidar validation became possible in early 2019. On 5 and 6 February 2019 a side-by-side instrument
239   comparison took place at Garmisch-Partenkirchen as a contribution to the FIRMOS (Far-Infrared Radiation
240   Mobile Observation System) validation project of the European Space Agency (Palchetti et al., 2021; Di Natale
241   et al., 2021). Two of the three balloons launched on 5 February were equipped with ozone sondes, while both
242   ballons on 6 February carried an ozone sonde. The ascents took place during night-time because of comparisons
243   of the CFH sondes with the water-vapour channel of the UFS Raman lidar that provides humidity profiles up to
244   at least 20 km (Klanner et al. 2021).

245   The first night of the campaign was clearer. The conditions for the comparison were excellent: the sondes rose

246   almost vertically up to 8.5 km and then slowly drifted to the south-east (Innsbruck), ideal for the comparison.

247   The balloons stayed within 20 km distance from IMK-IFU up to the tropopause (12.8 km a.s.l.) and remained

248   within 30 km up to 20 km a.s.l.

249   The launch times of the balloons were 18:03 CET (ascent to 16.147 km), 19:03 CET (29.475 km), and 23:00

250   CET (29.469 km).

251   In Fig. 2 we present the results of the four comparisons made. The measurements of lidar, ECC sonde and *in-situ*

252   sensor on 5 February are in outstanding agreement provided that a small constant offset is applied to the sonde

253   ozone between −0.53 and −3.4 ppb for the first three comparisons. The DIAL measurements are smoothed with a

254   numerical filter with an interval width growing with altitude (Trickl et al., 2020a). Nevertheless, the agreement

255   towards the tropopause is exceptional considering the low differential absorption for the wavelength pair 292

256   nm – 313 nm typically used above 6 km.

257   In addition, we show in Fig. 2 the results of three humidity measurements with the UFS Raman lidar (Klanner et

258   al., 2021) at a distance of 9 km from IMK-IFU. The water-vapour mixing ratios (MR) indicate a high variability

259   of the air composition between 5 and 8 km on both days, with a series of rapidly changing dry layers. In this

260   altitude range the MR do not agree quantitatively with those obtained with the CFH sondes. The MR of the lidar

261   is much less modulated because of the 1-h data-acquisition time necessary for the stratosphere. Because of this

262   variability the excellent air-mass matching by the side-by-side ozone soundings at IMK-IFU is crucial for the

263   results.

264   On 6 February the quality of the lidar retrievals was deteriorated by a layer of cirrus clouds above 9 km, which

265   required an aerosol correction. An increased level of ozone in this layer is remarkable, but is verified by the

266   sonde. By contrast, Reichardt et al. (1996) reported full ozone depletion in a cirrus layer that we traced back to

267   the surface of the Pacific Ocean where ozone destruction can be assumed to prevail (Kley et al., 1996). The

268   fourth comparison shows less perfect agreement because the lidar measurements ended at 19:00 CET, hours

269   before the last sonde ascent. This was the final measurement of the DIAL before its operation was terminated

270   after almost three decades.

271   Ozone profiles are also available for the descent of the balloons. The descents took place over Northern Italy and

272   intersected different air masses. As a consequence, strong discrepancies are seen, and we do not include these

273   data.

274   The first three comparisons yield average deviations of the sonde from the lidar. The average sonde offsets,

275   determined up to 5.8 km, were first subtracted from the sonde ozone values. Then, the differences between the

276   corrected sonde and the lidar data were formed at intervals of 52.5 m, for the first comparison on 6 February just

277   up to 8.7 km. Finally, these differences were averaged (Fig. 3). The agreement between the two systems without

278   the single-measurement offsets up to 9.2 km is ±2.5 ppb (about ±5 %). This is also the agreement we have found

279   between lidar and the mountain stations over the years and, thus, characterizes the winter-time performance of

280   the lidar after 2011.

281   The quality of the comparison shown in this section benefits from low to moderate ozone densities during the

282   cold season, which ensures limited absorption of the laser radiation within the troposphere. In Sect. 3.2 we assess

283   the performance for all seasons.

284

285

3.2 Comparison of MOHp ozone soundings with IFU lidar and *in-situ* measurements for 2018

The routine measurements with the IFU ozone DIAL exhibit rather different annual coverages, with gaps due to system damage or upgrading periods. Starting in late 2012 the final technical performance was reached. Retrieval strategies have been further improved. The best coverage of a single year was achieved in 2018 with a total of 587 measurements and 16 (March) to 79 (September) measurements per month. Therefore, we use this year for a thorough comparison with the MOHp ozone sonde.

The sonde ascents at MOHp usually take place around 6:00 CET on Monday, Wednesday and Friday, in summer just on Monday and Wednesday. We found a total of 46 of these days on which early-morning lidar measurements exist, not later than around 10:00 CET. On 36 of these days MOHp soundings are available. Thirteen of the days provided particularly good conditions with favourable temporal proximity. In the figures shown in this paper we eliminate ozone profiles for times later than 10:00 CET during a given day.

Winter

During the cold parts of the year the comparisons usually exhibit better quality. This is explained by less structured ozone vertical distributions and a wider operating range of the lidar due to the low ozone level allowing for a higher, less noisy far-field signal. This was already demonstrated in the previous section. For the 2018 comparison we give one example in Fig. 4. The lidar mixing ratio is of the order of 45 ppb, verified by the measurements at UFS (2660 m a.s.l.). The sonde results match the lidar values well if one adds 5.8 ppb. Just below the tropopause there is a minor discrepancy that could be either due to the higher uncertainty of the lidar measurement at these altitudes or air-mass differences.

Summer

During the warm season the ozone distribution in the middle and upper troposphere shows structured maxima caused by long-range transport, in particular STT (stratosphere-to-tropopause transport) layers (Trickl et al., 2020b). In this altitude range a summer maximum of STT exists. Usually, these structures do not perfectly match for both sites. An example for 9 July 2018 is shown in Fig. 5.

Figure 5 shows good agreement in structure between the soundings at both sites up to 9 km, in the presence of northerly advection. Again, the agreement was improved on the absolute scale by adding a correction to the sonde values (6 ppb). The elevated ozone between 3.3 km and 4.7 km can be explained by a stratospheric air intrusion, as is verified by the low RH. In the upper troposphere the agreement deteriorates, but at least the increase of ozone with altitude is seen in all profiles up to about 12 km. The ozone minimum around 13 km is just seen in the lidar data, with just a small ozone dip in the sonde profile. It is unreasonable to ascribe this considerable discrepancy to a temporary technical problem in such a limited altitude range. This example documents the difficulty of quantitative comparisons of tropospheric ozone even on a horizontal scale of just 38 km.

In order to clarify the origin of the difference of the ozone mixing ratio in the upper troposphere we calculated backward trajectories with the HYSPLIT model (http://ready.arl.noaa.gov/HYSPLIT.php; Draxler and Hess, 1998; Stein et al., 2015). These trajectories did not fully explain the observations due to the limited maximum backward time span of 315 h. This includes "ensemble" trajectory bundles that visualize a wider range of source regions.

Therefore, the trajectory calculations were extended to 350 h by using the LAGRANTO model for full-hour start times between 3:00 CET and 8:00 CET. Results for start times of 7:00 CET and 8:00 CET are shown in Figs. 6

326   and 7. Up to a start time of 4:00 CET the trajectories stayed almost completely at high altitudes. At 5:00 CET

327   three of the trajectories ended in the lower troposphere above the subtropical Pacific near a longitude of 180º,

328   first sign of an air-mass change. Later (Figs. 6 and 7) we see a clear influence of a Pacific source.

329   The low ozone level in the boundary layer above (sub)tropical oceans is well known (Eisele et al., 1999; Grant et

330   al., 2000; Trickl et al., 2003), in particular over the Pacific (Kley et al., 1996; Davies et al., 1998). In this way,

331   the lidar observations on 9 July 2018 can be understood. The launch time of the MOHp ozone sonde, 5:42 CET,

332   is between the two lidar measurements. However, a delay is caused by the northerly advection.

333   The moderate sonde RH indicates a potential admixture of aged stratospheric air above MOHp which would

334   explain the high ozone mixing ratios of more than 120 ppb.

335   Figures 5 and 8 show a rather constant negative ozone offset of the sonde profiles. The ozone profiles can be

336   brought into much better agreement by upward shifts by 6 ppb and 10 ppb, respectively. In Fig. 9 one sees one of

337   the very rare cases of a clear ozone mismatch between sonde and lidar up to elevations clearly above the

338   mountain sites (1 km above the Zugspitze summit). We conclude that differences between the Zugspitze sites

339   and the MOHp sonde are mostly not related to differences in air-composition in contrast to what was suspected

340   earlier.

341   The offsets of the MOHp data were evaluated for all 36 comparison days. The result is displayed in Fig. 10

342   where also the differences between the lidar results for 2671 m a.s.l. and the GAW measurements at UFS are

343   shown.

344   As found for the lidar measurements over many years (examples: Trickl et al., 2014, 2015, 2016, 2020b) the

345   lidar ozone agrees with that at UFS to within 2 to 3 ppb. The agreement would be better if orographic vertical

346   displacements and air flows on the ozone profiles would be considered (Carnuth et al., 2000; 2002; Yuan et al.,

347   2019). Orographic effects matter particularly in summer. Under warm conditions the lidar ozone seems to be

348   slightly higher on average with respect to UFS. A strong negative shift of −7 ppb can be seen in Fig. 5 where

349   UFS is located in the falling edge of a high-ozone range. This case was discarded from the statistical assessment.

350   The average difference between lidar and UFS for 2018 is 0.736 ppb ± 1.46 ppb (standard deviation). A positive

351   offset had also been found for an earlier four-day comparison with the Zugspitze summit, but with even higher

352   uncertainty (Trickl et al., 2020a). A positive offset of this size could be expected from the highly accurate cross-

353   section measurements of Viallon et al. (2015), who determined a negative bias of 1.8 % of the *in-situ* data

354   calibrated with the WMO standard. This relative difference becomes more important on the absolute scale in

355   summer than in winter because of the higher ozone values. It might explain the slight seasonal cycle of the

356   difference visible in Fig. 10. However, given the complex orography at the site we think that the uncertainties are

357   too high for such a conclusion.

358   The offsets between the MOHp sonde and the lidar are substantially higher. We exclude the lowest altitudes

359   from the comparison where obvious differences in ozone exist, e.g., due to local night-time ozone depletion

360   effects. The comparisons with the Zugspitze summit are mostly reasonable: Just in seven cases of the 36

361   comparisons for 2018 lower ozone in the sonde profiles reached up to more than 2.67 km (UFS), in three cases

362   to more than 3 km (Zugspitze summit). The offsets of the ozone sondes range from −12 ppb to + 4 ppb, with an

363   average of −3.77 ppb and a standard deviation of 4.22 ppb.

364   ***Differences***

365   In Figs. 11 to 13 we show average differences between lidar and offset-corrected MOHp sonde data as a function

366   of altitude and for three different ozone conditions, roughly below 50 ppb (low ozone), between 50 to 70 ppb

367 (moderate ozone) and more than 70 ppb (high ozone). The averaging was carried out just for measurement days
368 with lidar measurements in temporal proximity to the launch time of the ozone sonde. We also give the
369 percentages of the averages with respect to the offset-corrected sonde ozone. At high altitudes the sonde ozone is
370 a more useful reference than the lidar in the case of high ozone because of the considerable absolute uncertainty
371 caused by the loss of laser radiation.

372 For winter-type conditions (mixing ratio mostly less than 50 ppb) the six examples averaged exhibit low vertical
373 ozone structure which made the analysis straight forward and yields astonishingly small average differences
374 between 1 and 3 ppb. For moderate ozone and high ozone, mostly during the warm season, the vertical
375 distributions are more complex with changes on a time scale of even less than one hour. Here, we eliminated
376 several obvious ozone peaks and dips that differed at both stations. The six high-ozone cases were restricted to
377 July and August.

378 The averaged distributions of the differences exhibit oscillations. These oscillations were analysed for coherency
379 (not shown), but no systematic behaviour was identified. Thus, we ascribe the structure to noise. The noise
380 contains both an atmospheric and an instrumental component.

381 The noise amplitude shrinks above 6 km because of the change from 277 nm as the "on" wavelength to 292 nm.
382 This step is not clearly seen in Fig. 13 due to the higher 292-nm noise level. In July and August there are cases
383 with 100 to 150 ppb in the middle and upper troposphere. This can lead to lidar uncertainties even up to more
384 than 20 ppb during day-time because of the additional solar background noise. This is larger than the excursions
385 in the average in Fig. 13.

386 The analyses for 2018 do not reveal a significant bias between the lidar values and the offset-corrected sonde
387 data (based on the numbers underlying Fig. 10). The maximum noise excursions can be interpreted as maximum
388 combined uncertainties of lidar and sonde in a given altitude range. The results of this analysis confirm the
389 estimates in Table 4 of Trickl et al. (2020a).

390 **3.3 Comparisons of MOHp sonde, IFU lidar and *in-situ* measurements summits in 2009**

391 The results in Sect. 3.2 suggested to look also at a few earlier years. We select 2009 from the period of routine
392 measurements as another year of comparison. The lidar raw data were noisier than for the period after 2012 and
393 a tiny electronic ringing effect had to be removed mathematically. Thus, the uncertainties of the ozone profiles
394 above 6 km are higher than after the final system upgrading in 2012, particularly in summer. As a consequence,
395 a lidar validation is desirable at least for the upper troposphere. More importantly, in 2009 high-quality ozone
396 data still exist for the summit stations Wank (1780 m a.s.l.) and Zugspitze (2962 m a.s.l.). These stations benefit
397 from more frequent direct advection compared with UFS.

398 In 2009 the lidar was operated just until October which, nevertheless, allows us to make a reasonable number of
399 comparisons with MOHp. The operation was stopped afterwards since there were more and more cases of single-
400 bit errors in channel 5 of the transient digitizer system which had to be sent for repair. These errors induced
401 unrealistic data in the upper troposphere.

402 We identified a total of 23 days suitable for comparisons. On just eight of these days lidar measurements were
403 made in optimum temporal proximity. We find more deviations in the profiles than for 2018. In part, this can be
404 explained by atmospheric variability and insufficient air-mass matching. In addition, as mentioned, the raw data
405 of the lidar are noisier and some weak ringing had to be removed. This caused elevated uncertainties above 6
406 km. Nevertheless, the data allowed us to determine offsets for the MOHp ozone profiles, after verifying the data
407 quality of the lidar with the Zugspitze and Wank *in-situ* ozone.

408   In Fig. 14 we show the results of the analysis for 2009. The difference between IFU DIAL and Zugspitze is

409   −0.165 ppb ± 1.36 ppb (standard deviation), between DIAL and Wank +0.714 ppb ± 1.20 ppb. The DIAL ozone

410   below the Wank altitude is increasingly uncertain because of alignment issues of the near-field telescope. In an

411   earlier comparison for May 1999 (Trickl et al., 2020a) we selected a lower altitude in the DIAL data (2786 m)

412   and found better agreement, but, still, a slight positive offset with respect to the station. This is not attempted

413   here, although we can see the effect of orographic lifting in some examples.

414   For 2009 the offsets between DIAL and MOHp sondes were determined primarily by between 2 and 5 km. The

415   sonde offset obtained in this way is, again, negative on average (−1.500 ppb), with a standard deviation of 2.67

416   ppb, both being are less pronounced than in 2018.

417   Figure 15 shows a comparison on 12 January 2009, demonstrating excellent agreement between both systems,

418   except for the upper troposphere and lower stratosphere. In this case, the first lidar measurement took place at

419   9:20 CET, i.e., substantially later than the sonde ascent. Thus, the comparison has its limits. In the morning of 12

420   January westerly advection was revealed by HYSPLIT backward trajectories above at 7 km a.s.l.. This air mass

421   originated below 2 km over the subtropical. This could explain the slightly lower ozone level around this altitude

422   in the lidar results.

423   Another interesting example is August 17 (Fig. 16). The agreement between lidar and ozone sonde is highly

424   satisfactory up to 5.4 km and quite reasonable up to 10 km. However, between 10 km and 14.5 km the lidar

425   ozone is extremely low, in contrast to the sonde data. The pronounced ozone increase in the sonde data above 10

426   km is difficult to explain since the elevated RH values suggest neither a low tropopause nor the presence of a

427   stratospheric intrusion. On the other hand, the ozone peak above IMK-IFU descending roughly from 10 to 8 km

428   is attributed by HYSPLIT calculations to subsiding air, indicating the presence of an intrusion layer. It is

429   interesting that the rather short delay of the lidar measurements (7:00 CET to 9:15 CET) with respect to the

430   sonde ascent (launch time 5:57 CET) can result in such a considerable difference.

431   Again, 350-h LAGRANTO trajectories were calculated for start times above IMK-IFU between 3:00 CET and

432   8:00 CET (interval: 1 h) and start altitudes within the low-ozone layer. Until 6:00 CET the influence of marine

433   boundary layers is almost absent. Afterwards, the trajectories reveal a growing import from the first 600 m above

434   the subtropical Atlantic Ocean. In Fig. 17 the LAGRANTO results for 8:00 CET are shown.

435   In many cases the lidar seems to exhibit a negative bias with respect to the sondes in the upper troposphere. It is

436   advisable to re-examine a major part of the data between 2007 and 2011, also including strategies developed

437   later. For example, an exponential decay of the analogue signal was identified with the much lower noise of the

438   final setup (Trickl et al., 2020a) which must be addressed.

3.4 Comparisons of MOHp sonde, IFU lidar and *in-situ* measurements summits in 2000 and 2001

440   The period September 2000 to August 2001 is suitable for another comparison when a large number of STT-

441   related measurement series were made as a contribution to the STACCATO project (Stohl et al., 2003;

442   examples: Trickl et al., 2003; 2010; 2011; Zanis et al., 2003). These measurements were made with the detection

443   electronics of Eisele et al. (1999), but had the advantage that single-photon counting was used for the "solar

444   blind" "on" detection channels which added linearity above 5 km (starting in spring 1997). The counting system

445   was abandoned after 2003. A new one was installed after highly positive results in other IFU lidar systems in

446   2018 (Klanner et al., 2021), too late for routine operation.

447   The focus on STT during the STACCATO period made the comparisons a challenge because of the pronounced

448   layering. However, on 11 of the useful 20 days of comparison there was reasonable temporal proximity, due to

449 running long time series. The agreement between the lidar and the MOHp sonde was much better than expected
450 in the entire free troposphere. The agreement (after offset-correcting the MOHp profiles) is almost perfect during
451 the cold season. But also under high-ozone conditions the comparisons do not reveal systematic differences
452 beyond the sonde offsets.

453 Two examples for elevated ozone are shown in Figs. 18 and 19. The good comparisons support our earlier work
454 (Trickl et al., 2003, and 2010, respectively), and we tend to ascribe this to the good performance of the single-
455 photon counting system.

456 For several weeks a strange ozone rise towards the ground was observed in the lidar data below 1.5 km. This
457 effect disappeared after realigning the near-field telescope and the normal early-morning ozone drop returned.

458 However, the offsets of the MOHp mixing ratios necessary to achieve good agreement are, again, quite
459 substantial (Fig. 20). Also the differences between lidar and the stations are higher than those in the preceding
460 sections, and comparable with those of the mentioned four-day comparison for May 1999 (Trickl et al., 2020a).

461 The statistical analysis yields the following average differences and standard deviations:

462 IFU DIAL – Zugspitze: 1.22 ppb ± 1.81 ppb

463 IFU DIAL – Wank   −0.15 ppb ± 2.26 ppb

464 MOHp – IFU DIAL   −5.88 ppb ± 3.35 ppb

465 **4. Discussion and Conclusions**

466 For some time tropospheric differential-absorption ozone lidar systems had a bad reputation: The method is
467 highly sensitive to imperfections in the signal acquisition since the ozone number density is obtained by
468 derivative formation. In addition, a lidar covering the entire troposphere and the lowermost stratosphere features
469 a dynamic range of the backscatter signal of about eight decades, which means an extreme challenge for the
470 detection electronics.

471 Based on continual improvements, starting with the 1994 system upgrading, the IFU ozone DIAL gradually
472 approached a high performance until 2012, but there is, still, minor potential for improvements. Comparison
473 with the nearby mountain stations quite early demonstrated an uncertainty level of ±3 ppb in the lower
474 troposphere. Occasional comparisons with ozone sondes launched at the Hohenpeißenberg (1996 to 2001,
475 distance 38 km) were rather satisfactory up to the tropopause region.

476 Here, we more comprehensively analyse the lidar performance during three periods in its technical development.
477 The best agreement was found for the side-by-side comparison with balloon ascents of ozone sondes, performed
478 by the FZJ team at IMK-IFU in February 2019. Just a small, constant offset had to be subtracted from the sonde
479 data to achieve perfect agreement. For the more distant MOHp sonde the comparisons are more demanding
480 because of the high atmospheric variability (Vogelmann et al., 2011; 2015). This variability is particularly severe
481 in summer when the atmospheric layering is more pronounced. Nevertheless, there was enough agreement in
482 certain altitude ranges for examining the reliability of the ozone profiles obtained from the DIAL, also before the
483 final modifications in 2012. It turned out that just between 2007 and 2011 we can suspect a slight negative
484 summertime bias of the lidar of the order of 5 ppb above 6 km. This could be due to interfering structures on the
485 analogue signal (requiring mathematical correction) that could not be compensated by photon counting
486 (available just until 2003). In principle, this calls for a re-evaluation of the ozone profiles over the period 2007 to
487 2011, based on more recent experience in the signal inversion and the performance of the electronic equipment.

488 Vice versa, the lidar measurements helped us to identify the quality of the sonde measurements. Quite good
489 agreement can be achieved by applying an altitude-independent offset correction to the ozone values that

Atmospheric
Measurement
Techniques
Open Access

EGU

Discussions

490 strongly varies from sonde to sonde. In all but a few cases the offset can be determined to within ±2 ppb by a
491 comparison with the Zugspitze or the UFS station data. Most of the time differences in early-morning air-mass
492 composition between the two sites are limited to altitudes below 2 km. Thus, the differences reported earlier by
493 Scheel for 3 km (see introduction) are not caused by differences in air composition at both sites. A comparison
494 with the *in-situ* data is advisable despite the considerable distance between the sites.

495 The comparisons for the three years 2000-2001, 2009 and 2018 reveal just minor performance change of the
496 MOHp sonde over the years, with a variation of the annual average offset by about ±2 ppb. We found a negative
497 average offset of −3.64 ppb ± 3.72 ppb (standard deviation) with respect to the IFU ozone DIAL over all three
498 years. It is reasonable to assume that this offset is applicable to the entire tropospheric time series of the MOHp
499 sondes.

500 Remaining tasks for the lidar are a substantial reduction of the solar background at 313.2 nm in summer and to
501 enhance the moderate 291.8-nm backscatter signal in the upper troposphere. Further reduction of the residual
502 solar background is difficult since the spectral filtering is already quite narrow. However, replacement of the
503 rather aged (and partly contaminated) primary mirror of the far-field receiver could help by reducing the
504 background radiation reflected into the detection system. As mentioned longer averaging is advisable. By longer
505 averaging, the performance under low-aerosol conditions could almost reach that of *in-situ* measurements in a
506 major part of the troposphere. Single-photon counting can also be helpful for longer averaging times, as
507 demonstrated for our Raman lidar (Klanner et al., 2021). The noise level for counting is still lower than that of
508 the meanwhile outstanding transient digitizers (Trickl et al., 2020a).

509 **5 Data availability**

510 Lidar data and information on the lidar systems can be obtained on request from the IMK-IFU authors of this
511 paper (thomas@trickl.de, hannes.vogelmann@kit.edu). The 313-nm aerosol backscatter coefficients are archived
512 in the EARLINET data base, accessible through the ACTRIS data portal http://actris.nilu.no/. The
513 Hohenpeißenberg ozone and humidity data are stored in the NDACC data archive (https://www-
514 air.larc.nasa.gov/missions/ndacc/data.html#). The data of the FIRMOS campaign is available via the ESA
515 campaign dataset website https://earth.esa.int/eogateway/campaigns/firmos.

516 **6 Author statement**

517 TT carried out most lidar measurements after spring 1997, following U. Kempfer and H. Eisele. He led the
518 technical development of two ozone DIAL systems since 1990. HV was involved in the system upgrading since
519 2007 and was responsible for the lidar operation during FIRMOS. DC and CW launched several ECC sondes at
520 IMK-IFU in February 2019. MA and WS carried out the MOHp ozone sonde measurements. LR performed
521 Ozone *in-situ* measurements at the site Schneefernerhaus. MS provided LAGRANTO backward trajectories.

522 **7 Competing interests**

523 The authors declare that they have no conflict of interest.

Atmospheric
Measurement
Techniques
Discussions

541 **References**

542 ATMOFAST: Atmosphärischer Ferntransport und seine Auswirkungen auf die Spurengaskonzentrationen in der

543 freien Troposphäre über Mitteleuropa (Atmospheric Long-range Transport and its Impact on the Trace-gas

544 Composition of the Free Troposphere over Central Europe), Project Final Report, T. Trickl, co-ordinator, M.

545 Kerschgens, A. Stohl, and T. Trickl, subproject co-ordinators, funded by the German Ministry of Education and

546 Research within the programme "Atmosphärenforschung 2000", http://www.trickl.de/ATMOFAST.htm, 130

547 pp., 2005 (in German), with revised publication list of 2012

548 Ancellet, G., Pelon, J., Beekmann, M., Papayannis, A., and Mégie, G.: Ground-Based Lidar Studies of Ozone

549 Exchanges Between the Stratosphere and the Troposphere, J. Geophys. Res., 96, 22401-22421, 1991.

550 Ancellet, G., Godin-Beekmann, S., Smit, H. G. J., Stauffer, R. M., Van Malderen, R., Bodichon, R., and

551 Pazmiño, A.: Homogenization of the Observatoire de Haute Provence electrochemical concentration cell (ECC)

552 ozonesonde data record: comparison with lidar and satellite observations, Atmos. Meas. Tech., 15, 3105–3120,

553 2022.

554 Attmannspacher, W., and Dütsch, H.: 2nd International Ozone Sonde Intercomparison at the Observatory of

555 Hohenpeissenberg, Berichte des Deutschen Wetterdienstes 157, 1981.

556 Beekmann, M., Ancellet, G., Mégie, G., Snit, H. G. J., and Kley, D.: Intercomparison Campaign of Vertical

557 Ozone Profiles Including Electrochemical Sondes of ECC and Brewer-Mast Type and a Ground Based UV-

558 Differential Absorption Lidar, J. Atmos. Chem., 19, 259-288, 1994.

559 Brabec, M.: Backscatter and Humidity Measurements in Cirrus and Dust Clouds using Balloon Sondes, Ph.D.

560 thesis, Eidgenössische Technische Hochschule, Zürich (Switzerland), 96 pp., 2011.

561 Brewer, A. W., and Milford, J. R.: The Oxford-Kew ozone sonde, Proc. R. Soc. Lond. A, 256, 470–495

562 [available at http://doi.org/10.1098/rspa.1960.0120], 1960.

563 Browell, E. V., Danielsen, E. F., Ismail, S., Gregory, G. L., and Beck, S. M.: Tropopause Fold Structure

564 Determined From Airborne Lidar and in Situ Measurements, J. Geophys. Res., 92, 2112-2120, 1987.

565 Carnuth, W., and Trickl, T.: Transport studies with the IFU three-wavelength aerosol lidar during the VOTALP

566 Mesolcina experiment, Atmos. Environ., 34, 1425-1434, 2000.

567   Carnuth, W., Kempfer, U., and Trickl, T.: Highlights of the tropospheric lidar studies at IFU within the TOR
568   project, Tellus B, 54, 163-185, 2002.

569   Claude, H., Hartmannsgruber, R., and Köhler, U.: Measurement of atmospheric profiles using the Brewer-Mast
570   sonde, World Meteorological Organization, Global Ozone Res. and Monit. Proj. Report No. 17, WMO/TD No.
571   179, Geneva (Switzerland), [see also https://library.wmo.int/index.php?lvl=notice_display&id=11215], 51 pp.,
572   1987.

573   Deshler., T., Stübi, R., Schmidlin, F. J., Mercer, J. L., Smit, H. G. J., Johnson, B. J., Kivi, K., and Nardi, B.:
574   Methods to homogenize electrochemical concentration cell (ECC) ozonesonde measurements across changes in
575   sensing solution concentration or ozonesonde manufacturer, Atmos. Meas. Tech., 10, 2021–2043, 2017.

576   Daumont, D., Brion, J., Charbonnier, J., and Malicet, J.: Ozone UV Spectroscopy I: Absorption Cross-Sections
577   at Room Temperature, J. Atmos. Chem., 15, 145-155, 1992.

578   Davies, W. E., Vaughan, G., and O´Connor, F. M.: Observation of near-zero ozone concentrations in the upper
579   troposphere at mid-latitudes, Geophys. Res. Lett., 25, 1173-1176, 1998.

580   De Backer, H., De Muer, D., and De Sadelaer G.: Comparison of ozone profiles obtained with Brewer-Mast and
581   Z-ECC   sensors   during   simultaneous   ascents,   J.   Geophys.   Res.,   103,   19,641–19,648,
582   https://doi.org/10.1029/98JD01711 , 1998.

583   De Muer, D., and Malcorps, H.: The frequency response of an electrochemical ozone sonde and its application to
584   the deconvolution of ozone profiles, J. Geophys. Res., 89, 1361–1372, 1984.

585   Di Natale, G., Barucci, M., Belotti, C., Bianchini, G., D'Amato, F., Del Bianco, S. Gai, M., Montori, A.,
586   Sussmann, R., Viciani, S., Vogelmann, H., and Palchetti, L.: Comparison of mid-latitude single- and mixed-
587   phase cloud optical depth from co-located infrared spectrometer and backscatter lidar measurements, Atmos.
588   Meas. Tech., 14, 6749–6758, 2021.

589   Dirksen, R. J., Sommer, M., Immler, F. J., Hurst, D. F., Kivi, R., and Vömel, H.: Reference quality upper-air
590   measurements: GRUAN data processing for the Vaisala RS92 radiosonde, Atmos. Meas. Tech., 7, 4463-4490,
591   doi.org/10.5194/amt-7-4463-2014, 2014.

592   Draxler, R., and Hess, G.: An overview of the HYSPLIT_4 modelling system for trajectories, dispersion, and
593   deposition, Aust. Meteorol. Mag., 47, pp. 295-308, 1998.

594   Eisele, H., Trickl, T., and Claude, H.: Lidar als wichtige Ergänzung zur Messung troposphärischen Ozons,
595   Ozonbulletin des Deutsches Wetterdiensts, 44, 2 pp., 1997 (in German).

596   Eisele, H., Scheel, H. E., Sladkovic, R., and Trickl, T.: High-Resolution Lidar Measurements of Stratosphere-
597   Troposphere Exchange, J. Atmos. Sci., 56, 319-330, 1999.

598   Eisele, H., and Trickl, T.: Improvements of the aerosol algorithm in ozone-lidar data processing by use of
599   evolutionary strategies, Appl. Opt., 44, 2638-2651, 2005.

600   EUROTRAC: Transport and Chemical Transformation of Pollutants in the Troposphere, Vol. 1, An Overview of
601   the Work of EUROTRAC, P. Borrell and P. M. Borrell, Eds., Springer (Berlin, Heidelberg, New York), ISBN 3-
602   540-66775-X, 474 pp., 1997.

603   Gaudel, A., Ancellet G., and Godin-Beekmann S.: Analysis of 20 years of tropospheric ozone vertical profiles by
604   lidar and ECC at Observatoire de Haute Provence (OHP) at 44° N, 6.7° E, Atmos. Environ., 113, 78-89, 2015.

605   Gaudel, A., Cooper, O. R., Ancellet, G., Barret, B., Boynard, A., Burrows, J. P., Clerbaux, J. P., Coheur, P.-F.,
606   Cuesta, J., Cuevas, E., Doniki, S., Dufour, G., Ebojie, F., Foret, G., Garcia, O., Granados-Muñoz, M. J.,
607   Hannigan, J., Hase, F., Hassler, B., Huang, G., Hurtmans, D., Jaffe, D., Jones, N., Kalabokas, P., Kerridge, B.,
608   Kulawik, S., Latter, B., Leblanc, T., Le Flochmoën, E., Lin, W., Liu, J., Liu, X., Mahieu, E., McClure-Begley,
609   A., Neu, J., Osman, M., Palm, M., Petetin, H., Petropavlovskikh, I., Querel, R., Rahpoe, N., Rozanov, A.,
610   Schultz, M. G., Schwab, J., Siddans, R., Smale, D., Steinbacher, M., Tanimoto, H., Tarasick, D., Thouret, V.,
611   Thompson, A., M., Trickl, T., Weatherhead, E., Wespes, C., Worden, H., Vigouroux, C., Xu, X., Zeng, G.,
612   Ziemke, J.: Tropospheric Ozone Assessment Report: Present-day distribution and trends of tropospheric ozone
613   relevant to climate and global atmospheric chemistry model evaluation, Elem. Sci. Anth., 6, 39, DOI:
614   https://doi.org/ 10.1525/elementa.291, 58 pp., 2018.

615   Grant, W. B., Browell, E. V., Butler, C. F., Fenn, M. A., Clayton, M. B., Hannan, J. R., Fuelberg, H. E., Blake,
616   D. R., Blake, N. J., Gregory, G. L., Heikes, B. G., Sachse, G. W., Singh, H. B., Snow, J., and Talbot, R. W.: A
617   case study of transport of tropical marine boundary layer and lower tropospheric air masses to the northern
618   midlatitude upper troposphere, J. Geophys. Res., 105, 3757-3769, 2000.

619   Hearn, A. G.: The Absorption of Ozone in the Ultra-violet and Visible Regions of the Spectrum, Proc. Phys.
620   Soc., 78, 932-940, 1961.

621   Hersbach, H, Bell, B, Berrisford, P, Simmons, A., Berrisford, P., Dahlgren, P., Horanyi, A., Munoz-Sabater, J.,
622   Nicolas, J., Radu, R., Schepers, D., Soci, C., Villaume, S., Bidlot, J. R., Haimberger, L.; Woollen, J.,
623   Buontempo, C., and Thepaut, J. N.: The ERA5 global reanalysis. Q. J. R. Meteorol Soc., 146, 1999– 2049,
624   https://doi.org/10.1002/qj.3803, 2020.

625   Johnson, B. J., Oltmans, S. J., Vömel, H., Smit, H. G. J., Deshler, T., and Kröger, C.: Electrochemical
626   concentration cell (ECC) ozonesonde pump efficiency measurements and tests on the sensitivity to ozone of
627   buffered and unbuffered ECC sensor cathode solutions, J. Geophys. Res.-Atmos., 107, ACH 8-1–ACH 8-18,
628   https://doi.org/10.1029/2001JD000557, 2002.

629   Jeannet, P., Stübi, R., Levrat, G., Viatte, P., and J. Staehelin, J.: Ozone balloon soundings at Payerne
630   (Switzerland): Reevaluation of the time series 1967–2002 and trend analysis, J. Geophys. Res., 112, D11302,
631   doi:10.1029/2005JD006862, 15 pp., 2007.

632   Kempfer, U., Carnuth, W., Lotz, R., and Trickl, T.: A wide range ultraviolet lidar system for tropospheric ozone
633   measurements: development and application, Rev. Sci. Instrum., 65, 3145-3164, 1994.

634   Kerr, J. B., Fast, H., McElroy, C.T., Oltmans, S.J., Lathrop, J.A., Kyro, E., Paukkunen, A., Claude, H., Köhler,
635   U., Sreedharan, C.R., akao T., and Tsukagoshi, Y.: The 1991 WMO International Ozonesonde Intercomparison
636   at Vanskoy, Canada. Atmos.–Ocean, 32, 685–716, https://doi.org/10.1080/07055900.1994.9649518, 1994.

637   Klanner, L., Höveler, K., Khordakova, D., Perfahl, M., Rolf, C., Trickl, T., and Vogelmann, H.: A powerful lidar
638   system capable of 1 h measurements of water vapour in the troposphere and the lower stratosphere as well as the
639   temperature in the upper stratosphere and mesosphere, Atmos. Meas. Tech., 14, 531-555, 2021.

640   Klausen, J., Zellweger, C., Buchmann, B., and Hofer, P.: Uncertainty and bias of surface ozone measurements at
641   selected Global Atmospheric Watch sites, J. Geophys. Res., 108, 4622, doi: 10.1029/2003JD003710, 17 pp.,
642   2003.

Atmospheric
Measurement
Techniques
Discussions

Open Access

EGU

643 Kley, D., Beck, J., Grennfelt, P. I., Hov, O., and Penkett, S. A.: Tropospheric Ozone Research (TOR) A Sub-
644 Project of EUROTRAC, J. Atmos. Chem., 28, 1–9, 1997.

645 Kley, D., Crutzen, P. J., Smit, H. G. J., Vömel, H., Oltmans, S., Grassl, H., and Ramanathan, V.: Observations of
646 Near-Zero Ozone Concentrations Over the Convective Pacific: Effects on Air Chemistry, Science, 274, 230-233,
647 1996.

648 Komhyr, W.D.: Electrochemical concentration cells for gas analysis, Ann. Geoph., 25, 203–210, 1969.

649 Komhyr, W. D., Barnes, R. A., Brothers, G. B., Lathrop, J. A., and Opperman, D. P.: Electrochemical
650 concentration cell ozonesonde performance evaluation during STOIC 1989, J. Geophys. Res., 100, 9231–9244,
651 https://doi.org/10.1029/94JD02175, 1995.

652 Langford, A. O., Masters, C. D., Proffitt, M. H., Hsie, E.-Y., and Tuck, A. F.: Ozone measurements in a
653 tropopause fold associated with a cut-off low system, Geophys. Res. Lett., 23, 2501–2504, 1996.

654 Logan, J.A., Staehelin, J., Megretskaia, I.A., Cammas, J.-P., Thouret, V., Claude, H., De Backer, H.,
655 Steinbacher, M., Scheel, H.-E., Stübi, R., Fröhlich, M., and Derwent, R. (2012), Changes in ozone over Europe:
656 Analysis of ozone measurements from sondes, regular aircraft (MOZAIC) and alpine surface sites, J. Geophys.
657 Res., 117, D09301, doi:10.1029/2011JD016952.

658 Malicet, J., Daumont, D., Charbonnier, J., Parisse, C., Chakir, A., and Brion, J.: Ozone UV Spectroscopy I:
659 Absorption Cross-Sections and Temperature Dependence, J. Atmos. Chem., 21, 263-273, 1995.

660 Palchetti, L., Barucci, M., Belotti, C., Bianchini, G., Cluzet, B., D'Amato, F., Del Bianco, S., Di Natale, G., Gai,
661 M., Khordakova, D., Montori, A., Oetjen, H., Rettinger, M., Rolf, C., Schuettemeyer, D., Sussmann, R., Viciani,
662 S., Vogelmann, H., and Wienhold, F. G.: Observations of the downwelling far-infrared atmospheric emission at
663 the Zugspitze observatory, Earth Syst. Sci. Data, 13, 4303–4312, https://doi.org/10.5194/essd-13-4303-2021,
664 2021.

665 Schultz, M. G., Schröder, S., Lyapina, O., Cooper, O., Galbally, I., Petropavlovskikh, I., von Schneidemesser,
666 E., Tanimoto, H., Elshorbany, Y., Naja, M., Seguel, R. J., Dauert, U., Eckhardt, P., Feigenspan, S., Fiebig, M.,
667 Hjellbrekke, A.-G., Hong, Y.-D., Kjeld, P. C., Koide, H., Lear, G., Tarasick, D., Ueno, M., Wallasch, M.,
668 Baumgardner, D., Chuang, M.-T., Gillett, R., Lee, M., Molloy, S., Moolla, R., Wang, T., Sharps, K., Adame, J.
669 A., Ancellet, G., Apadula, F., Artaxo, P., Barlasina, M. E., Bogucka, M., Bonasoni, P., Chang, L., Colomb, A.,
670 Cuevas-Agulló, E., Cupeiro, M., Degorska, A., Ding, A., Fröhlich, M., Frolova, M., Gadhavi, H., Gheusi, F.,
671 Gilge, S., Gonzalez, M. Y., Gros, V., Hamad, S. H., Helmig, D., Henriques, D., Hermansen, O., Holla, R.,
672 Hueber, J., Im, U., Jaffe, D. A., Komala, N., Kubistin, D., Lam, K.-S., Laurila, T., Lee, H., Levy, I., Mazzoleni,
673 C., Mazzoleni, L. R., McClure-Begley, A., Mohamad, M., Murovec, M., Navarro-Comas, M., Nicodim, F.,
674 Parrish, D., Read, K. A., Reid, N., Ries, L., Saxena, P., Schwab, J. J., Scorgie, Y., Senik, I., Simmonds, P.,
675 Sinha, V., Skorokhod, A. I., Spain, G., Spangl, W., Spoor, R., Springston, S. R., Steer, K., Steinbacher, M.,
676 Suharguniyawan, E., Torre, P., Trickl, T., Weili, L., Weller, R., Xiaobin, X., Xue, L., and Zhiqiang, M.:
677 Tropospheric Ozone Assessment Report: Database and Metrics Data of Global Surface Ozone Observations,
678 Elem. Sci. Anth., 5, 58, DOI: https://doi.org/ 10.1525/elementa.244, 25 pp., 2017.

679 Reichardt, J., Ansmann, A., Serwazi, M., Weitkamp, C., and Michaelis, W.: Unexpectedly low ozone
680 concentration in midlatitude tropospheric ice clouds: A case study, Geophys. Res.Lett., 23, 1929-1932, 1996.

Atmospheric
Measurement
Techniques
Discussions

681   Smit, H. G. J, Straeter, W., Johnson, B. J., Oltmans, S. J., Davies, J., Tarasick, D. W., Hoegger, B., Stubi, R.,
682   Schmidlin, F. J., Northam, T., Thompson, A. M., Witte, J. C., Boyd, I., and Posny, F.: Assessment of the
683   Performance of ECC-ozonesondes under Quasi-flight Conditions in the Environmental Simulation Chamber:
684   Insights from the Jülich Ozone Sonde Intercomparison Experiment (JOSIE), J. Geophys. Res., 112, D19306,
685   doi:10.1029/2006JD007308, 18 pp., 2007.

686   Smit, H.G.J., and ASOPOS panel: Quality assurance and quality control for ozonesonde measurements in GAW,
687   World Meteorological Organization, GAW Report No. 201, Geneva (Switzerland). [Available online at
688   https://library.wmo.int/doc_num.php?explnum_id=7167], 100 pp., 2014.

689   Smit, H.G.J., and Thompson, A.M.: Ozonesonde Measurement Principles and Best Operational Practices:
690   ASOPOS 2.0 (Assessment of Standard Operating Procedures for Ozonesondes), World Meteorological
691   Organization, GAW Report No. 268, Geneva (Switzerland). [Available online at
692   https://library.wmo.int/doc_num.php?explnum_id=10884], 172 pp., 2021.

693   Stauffer, R.M., Thompson, A.M., Kollonige, D.E., Tarasick, D.W., Van Malderen, R., Smit, H.G.J., Vömel, H.,
694   Morris, G.A., Johnson, B.J., Cullis, P.D., Stübi, R., Davies, J., and Yan.: An Examination of the Recent Stability
695   of Ozonesonde Global Network Data, Earth and Space Science, 9 (10), e2022EA002459, [available online at
696   https://doi.org/10.1029/2022EA002459], 2022.

697   Stein, A. F., Draxler, R. R, Rolph, G. D., Stunder, B. J. B., Cohen, M. D., and Ngan, F.: NOAA's HYSPLIT
698   atmospheric transport and dispersion modeling system, Bull. Amer. Meteor. Soc., 96, 2059-2077, 2015.

699   Steinbrecht, W., Schwarz, R., and Claude, H.: New pump correction for the Brewer-Mast ozone sonde:
700   determination from experiment and instrument intercomparisons, J. Atmos. Ocean. Tech., 15, 144–156, 1998.

701   Stohl, A., and Trickl, T.: A textbook example of long-range transport: Simultaneous observation of ozone
702   maxima of stratospheric and North American origin in the free troposphere over Europe, J. Geophys. Res., 104,
703   30445-30462, 1999.

704   Stohl, A., Bonasoni, P., Cristofanelli, P., Collins, W., Feichter, J., Frank, A., Forster, C., Gerasopoulos, E.,
705   Gäggeler, H., James, P., Kentarchos, T., Kromp-Kolb, H., Krüger, B., Land, C., Meloen, J., Papayannis, A.,
706   Priller, A., Seibert, P., Sprenger, M., Roelofs, G. J., Scheel, H. E., Schnabel, C., Siegmund, P., Tobler, L., Trickl,
707   T., Wernli, H., Wirth, V., Zanis, P., and Zerefos, C.: Stratosphere-troposphere exchange - a review, and what we
708   have learned from STACCATO, J. Geophys. Res., 108, 8516, doi:10.1029/2002JD002490, STA 1, 15 pp., 2003.

709   Stübi, R., Levrat, G., Hoegger, B., Pierre Viatte, P., Staehelin, J., Schmidlin, F.J.: In-flight comparison of
710   Brewer-Mast and electrochemical concentration cell ozonesondes, J. Geophys. Res., 113, D13302,
711   https://doi.org/10.1029/2007JD009091 , 2008.

712   Tarasick, D. W., Davies, J., Anlauf, K., Watt, M., Steinbrecht, W., Claude H.-J.: Laboratory investigations of the
713   response of Brewer-Mast ozonesondes to tropospheric ozone, J. Geophys. Res., 107, ACH 14-1 – 14-10,
714   https://doi.org/10.1029/2001JD001167 , 2002.

715   Tarasick, D. W., Davies, J., Smit, H. G. J., and Oltmans, S. J.: A re-evaluated Canadian ozonesonde record:
716   measurements of the vertical distribution of ozone over Canada from 1966 to 2013, Atmos. Meas. Tech., 9, 195–
717   214, https://doi.org/10.5194/amt-9-195-2016, 2016.

718   Tarasick, D., Galbally, I. E., Cooper, O. R., Schultz, G M., Ancellet, G., Leblanc, T., Wallington, T. J., Ziemke,
719   J., Liu, X., Steinbacher, M., Staehelin, J., Vigouroux, C., Hannigan, J., García, O., Foret, G., Zanis, P.,

720   Weatherhead, E., Petropavlovskikh, I., Worden, H., Osman, M., Liu, J., Chang, K.-L., Gaudel, A., Lin, M.,
721   Granados-Muñoz, M., Thompson, A. M., Oltmans, S. J., Cuesta, J., Dufour, G., Thouret, V., Hassler, B., Trickl,
722   T., and Neu, J. L.: Tropospheric Ozone Assessment Report: Tropospheric ozone from 1877 to 2016, observed
723   levels, trends and uncertainties, Elem. Sci. Anth., **7**, Article 39, DOI: https://doi.org/10.1525/elementa.376, 72
724   pp. (plus 56 pp. of supplemental material), 2019.

725   Tarasick, D. W., Smit, H. G. J., Thompson, A. M., Morris, G. A., Witte, J. C., Davies, J., Davies, J., Nakano, T.,
726   Van Malderen, R., Stauffer, R. M., Johnson, B. J., Stubi1, R., Oltmans, S. J., and Vömel, H.: Improving ECC
727   ozonesonde data quality: Assessment of current methods and outstanding issues, Earth and Space Science, 8,
728   e2019EA000914. https://doi.org/10.1029/2019EA000914, 27 pp., 2021.

729   TESLAS: Tropospheric Environmental Studies by Laser Sounding (TESLAS), in: Transport and Chemical
730   Transformation of Pollutants in the Troposphere, Vol. 8, Instrument Development for Atmospheric Research and
731   Monitoring, J. Bösenberg, D. Brassington, and P. C. Simon, Eds., Springer (Berlin, Heidelberg, New York),
732   ISBN 3-540-62516-X, 1-203, 1997.

733   Thompson, A. M., Smit, H. G. J., Witte, J. C., Stauffer, R. M., Johnson, B. J., Morris, G., von der Gathen, P.,
734   Van Malderen, R., Davies, J., Piters, A., Allaart, M., Posny, F., Kivi, R., Cullis, P., Hoang Anh, N. T., Corrales,
735   E., Machinini, T., da Silva, F. R., Paiman, G., Thiong'o, K., Zainal, Z., Brothers, G. B., Wolff, K. R., Nakano,
736   T., Stübi, R., Romanens, G., Coetzee, G. J. R., Diaz, J. A., Mitro, S., Mohamad, M., and Ogino, S.: Ozonesonde
737   Quality Assurance: The JOSIE–SHADOZ (2017) Experience, Bulletin of the American Meteorological Society,
738   100, 155-171, 2019.

739   Trickl, T., Cooper, O. R., Eisele, H., James, P., Mücke, R., and Stohl, A.: Intercontinental transport and its
740   influence on the ozone concentrations over central Europe: Three case studies, J. Geophys. Res., 108, D12, 8530,
741   10.1029/2002JD002735, STA 15, 23 pp., 2003.

742   Trickl, T., Feldmann, H., Kanter, H.-J., Scheel, H. E., Sprenger, M., Stohl, A., and Wernli, H.: Deep
743   stratospheric intrusions over Central Europe: case studies and climatological aspects, Atmos. Chem. Phys., 10,
744   499-524, 2010.

745   Trickl, T., Eisele, H., Bärtsch-Ritter, N., Furger, M., Mücke, R., Sprenger, M., and Stohl, A.: High-ozone layers
746   in the middle and upper troposphere above Central Europe: potential import from the stratosphere along the
747   subtropical jet stream, Atmos. Chem. Phys., 11, 9343-9366; 5-p. Supplement, 2011.

748   Trickl, T., Vogelmann, H., Giehl, H., Scheel, H. E., Sprenger, M., and Stohl, A.: How stratospheric are deep
749   stratospheric intrusions? Atmos. Chem. Phys., 14, 9941-9961, 2014.

750   Trickl, T., Vogelmann, H., Flentje, H., and Ries, L.: Stratospheric ozone in boreal fire plumes – the 2013 smoke
751   season over Central Europe, Atmos. Chem. Phys., 15, 9631-9649, 2015.

752   Trickl, T., Vogelmann, H., Fix, A., Schäfler, A., Wirth, M., Calpini, B., Levrat, G., Romanens, G., Apituley, A.,
753   Wilson, K. M., Begbie, R., Reichardt, J., Vömel, H. and Sprenger, M.: How stratospheric are deep stratospheric
754   intrusions into the troposphere? LUAMI 2008, Atmos. Chem. Phys, 16, 8791-8815, 2016.

755   Trickl, T., Neidl, F., Giehl, H., Perfahl, M., and Vogelmann, H.: Three decades of tropospheric ozone lidar
756   development at Garmisch-Partenkirchen, Atmos. Meas. Tech., 13, 6357-6390, 2020a.

757   Trickl, T., Vogelmann, H., Ries, L., and Sprenger, M.: Very high stratospheric influence observed in the free
758   troposphere over the Northern Alps – just a local phenomenon? Atmos. Chem. Phys., 20, 243-266, 2020b.

Atmospheric
Measurement
Techniques
Open Access

Discussions

EGU

759   Vaisala: Vaisala Radiosonde RS41 Measurement Performance, White Paper, Vaisala, Helsinki (Finland),
760   https://www.vaisala.com/sites/default/files/documents/WEA-MET-RS41-Performance-White-paper-
761   B211356EN-B-LOW-v3.pdf, 28 pp. (accessed 7 September 2019), 2017.

762   Van Malderen, R., Allaart, M. A. F., De Backer, H., Smit, H. G. J., and De Muer, D.: On instrumental errors and
763   related correction strategies of ozonesondes: possible effect on calculated ozone trends for the nearby sites Uccle
764   and De Bilt, Atmos. Meas. Tech., 9, 3793–3816, 2016

765   Viallon, J., Lee, S., Moussay, P., Tworek, K., Peterson, M., and Wielgosz, R. I.: Accurate measurements of
766   ozone absorption cross-sections in the Hartley band, Atmos. Meas. Tech., 8, 1245-1257, 2015.

767   Völger, P., Bösenberg, J., and Schult, I.: Scattering Properties of Selected Model Aerosols Calculated at UV-
768   Wavelengths: Implications for DIAL Measurements of Tropospheric Ozone, Beitr. Phys. Atmosph., 69, 177-
769   187, 1996.

770   Vömel, H., David, D. E., and Smith, K.: Accuracy of tropospheric and stratospheric water vapor measurements
771   by the cryogenic frost point hygrometer: Instrumental details and observations, J. Geophys. Res., 112, D08305,
772   doi: 10.1029/2006JD007224, 14 pp., 2007.

773   Vömel, H., Naebert, T., Dirksen, R., and Sommer, M.: An update on the uncertainties of water vapor
774   measurements using Cryogenic Frostpoint Hygrometers, Atmos. Meas. Tech., 9, 3755-3768, 2016.

775   Vömel, H., Smit, H. G. J., Tarasick, D., Johnson, B., Oltmans, S. J., Selkirk, H., Thompson, A. M., Stauffer, R.
776   M., Witte, J. C., Davies, J., van Malderen, R., Morris, G. A., Nakano, T., and Stübi, R.: A new method to correct
777   the electrochemical concentration cell (ECC) ozonesonde time response and its implications for "background
778   current" and pump efficiency, Atmos. Meas. Tech., 13, 5667–5680, 2020.

779   Vogelmann, H. and Trickl, T.: Wide-Range Sounding of Free-Tropospheric Water Vapor with a Differential-
780   Absorption Lidar (DIAL) at a High-Altitude Station, Appl. Opt., 47, 2116-2132, 2008.

781   Vogelmann, H., Sussmann, R., Trickl, T., and Borsdorff, T.: Intercomparison of atmospheric water vapor
782   soundings from the differential absorption lidar (DIAL) and the solar FTIR system on Mt. Zugspitze, Atmos.
783   Meas. Tech., 4, 835-841, 2011.

784   Vogelmann, H., Sussmann, R., Trickl, T., and Reichardt, A.: Spatiotemporal variability of water vapor
785   investigated using lidar and FTIR vertical soundings above the Zugspitze, Atmos. Chem. Phys., 14, 3135-3148,
786   2015.

787   VOTALP II: Vertical Ozone Transport in the Alps II, Final Report for the European Union, Contract Nr.: ENV4
788   CT970413, Reporting Period 1/3/1998-29/2/2000, H. Kromp-Kolb, Co-ordinator, Universität für Bodenkultur
789   Wien (Austria), Institut für Meteorologie und Physik, 96 pp., 2000.

790   Wernli, H., and Davies, H.C.: A Lagrangian-based analysis of extratropical cyclones. I: The method and some
791   applications. Q.J.R. Meteorol. Soc., 123: 467-489, https://doi.org/10.1002/qj.49712353811, 1997.

792   Sprenger, M., and Wernli, H.: The LAGRANTO Lagrangian analysis tool – version 2.0, Geosci. Model Dev., 8,
793   2569–2586, https://doi.org/10.5194/gmd-8-2569-2015, 2015.

794   Wotava, G., and Kromp-Kolb, H.: The research project VOTALP – general objectives and main results, Atmos.
795   Environ., 34, 1319-1322, 2000.

796   Yuan, Y., Ries, L., Petermeier, H., Trickl, T., Leuchner, M., Couret, C., Sohmer, R., Meinhardt, F., and Menzel,

797   A.: On the diurnal, weekly, and seasonal cycles and annual trends in atmospheric CO_2 at Mount Zugspitze,

798   Germany, during 1981–2016, Atmos. Chem. Phys., 19, 999–1012, https://doi.org/10.5194/acp-19-999-2019,

799   2019.

800   Zanis, P., Trickl, T., Stohl, A., Wernli, H., Cooper, O., Zerefos, C., Gaeggeler, H., Priller, A., Schnabel, C.,

801   Scheel, H. E., Kanter, H. J., Tobler, L., Kubik, P. W., Cristofanelli, P., Forster, C., James, P., Gerasopoulos, E.,

802   Delcloo, A., Papayannis, A., and Claude, H.: Forecast, observation and modelling of a deep stratospheric

803   intrusion event over Europe, Atmos. Chem. Phys., 3, 763-777, 2003.

804

805

Atmospheric
Measurement
Techniques
Discussions

806

807   **Figures:**

808
809
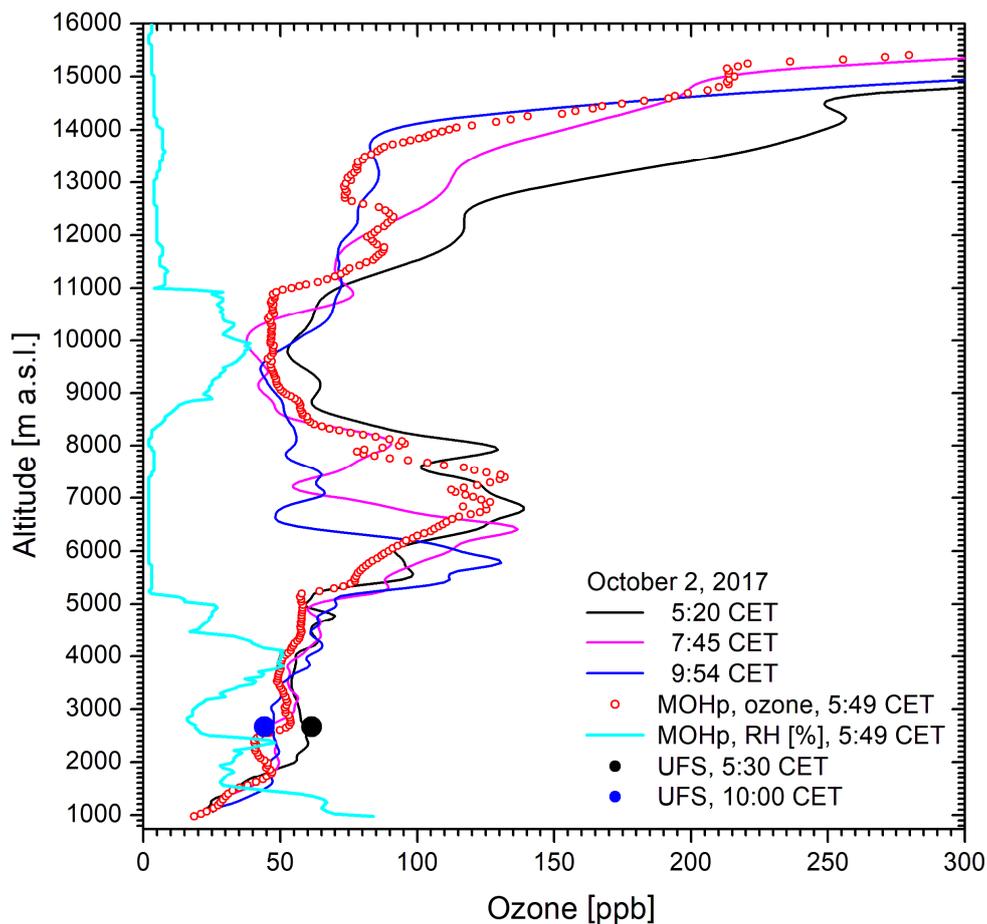
810   **Fig. 1.** Ozone measurements at Garmisch-Partenkirchen (IFU, UFS) and Hohenpeißenberg (MOHp) on 2
811   October 2017; the low relative humidity between 5.2 and 8.3 km (RH = 2 %) verifies the presence of a
812   stratospheric air intrusion. The time for MOHp is the launch time of the sonde.
813

814
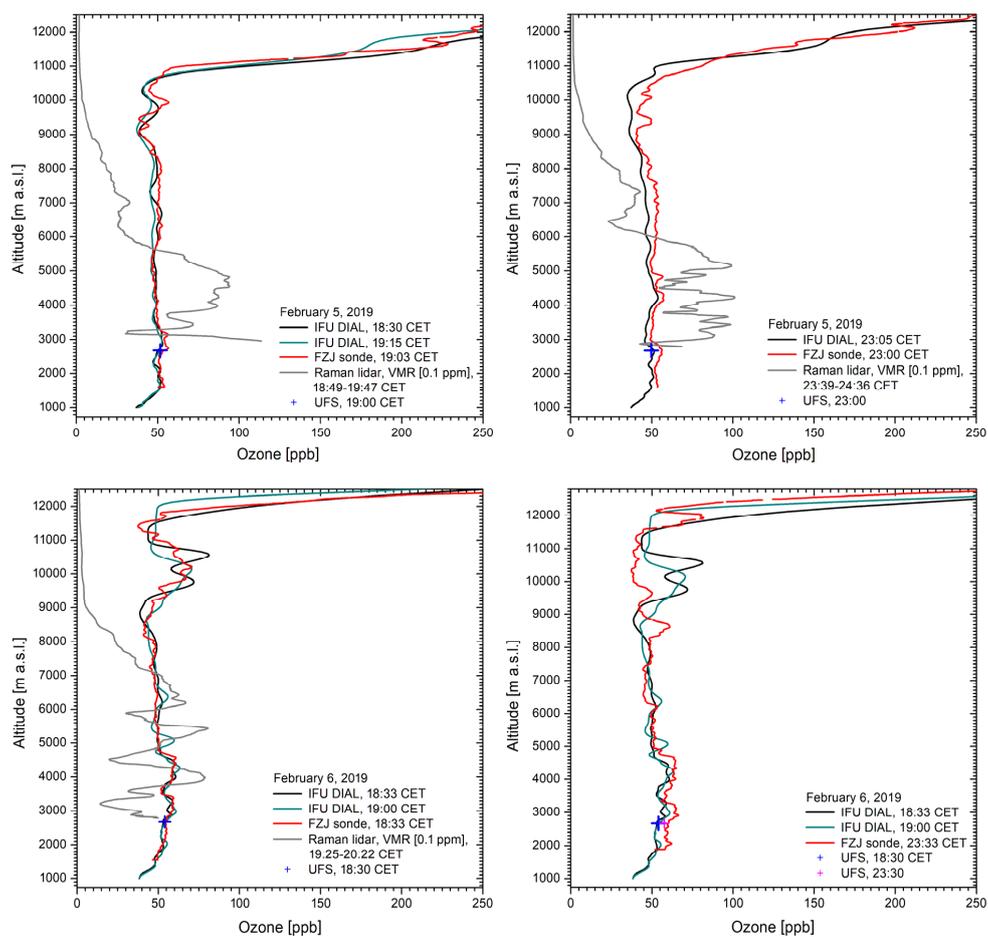
Fig. 2. Four ozone measurements on 5 and 6 February 2019 with lidar (IFU), ECC sonde (FZJ) and an *in-situ* sensor at UFS; for two measurements the FZJ ozone mixing ratios are slightly higher than the lidar results. The fourth FZJ ozone measurement took place much later than the final lidar measurements which resulted in slightly larger differences. The lidar results around 10 km on 6 February are uncertain due to a cirrus correction. In order to visualize more details on the layering we also show water-vapour mixing ratios for roughly co-inciding measurements of the UFS Raman lidar. The tropospheric structures are strongly smoothed due to the 1-h data-acquisition time.

Atmospheric
Measurement
Techniques
Discussions

Open Access

EGU

823
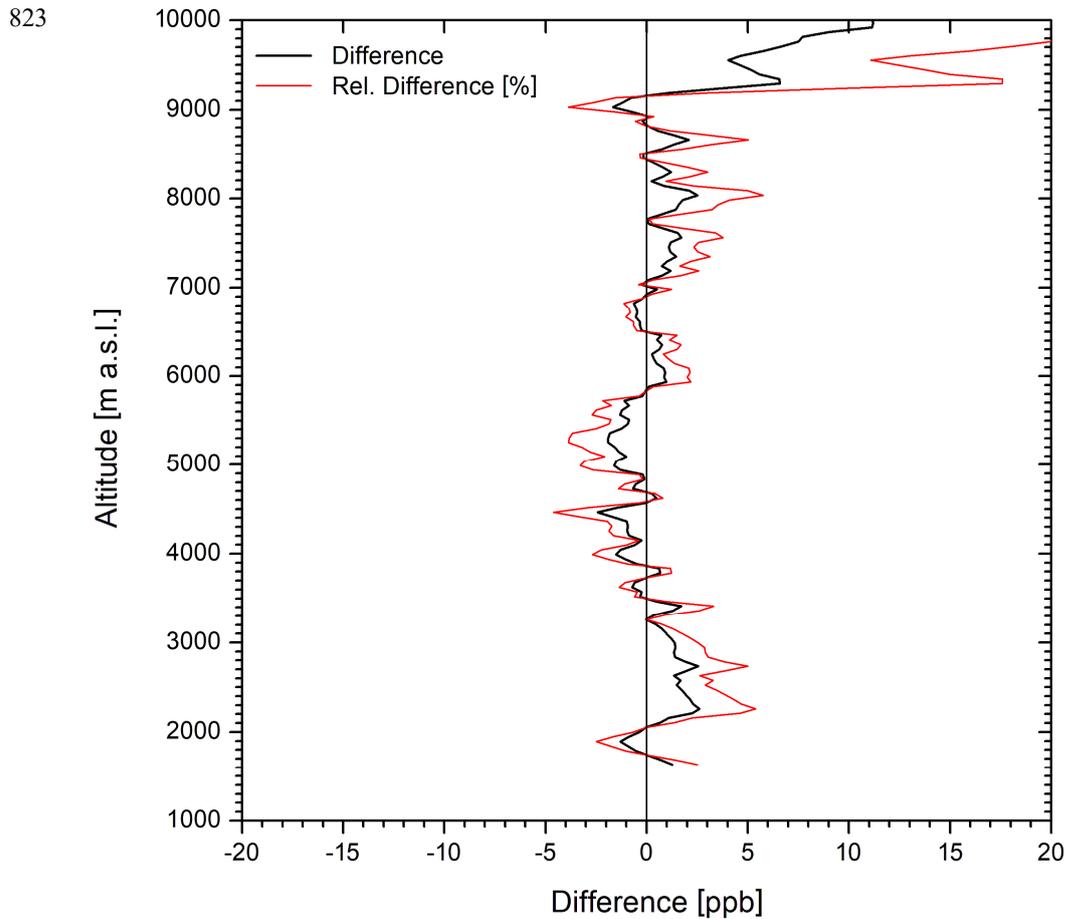
Fig. 3. Averaged differences between FZJ ozone sonde and IMK-IFU lidar for the first three comparisons after a

824

slight offset correction (see text)

825

826
827
828

829
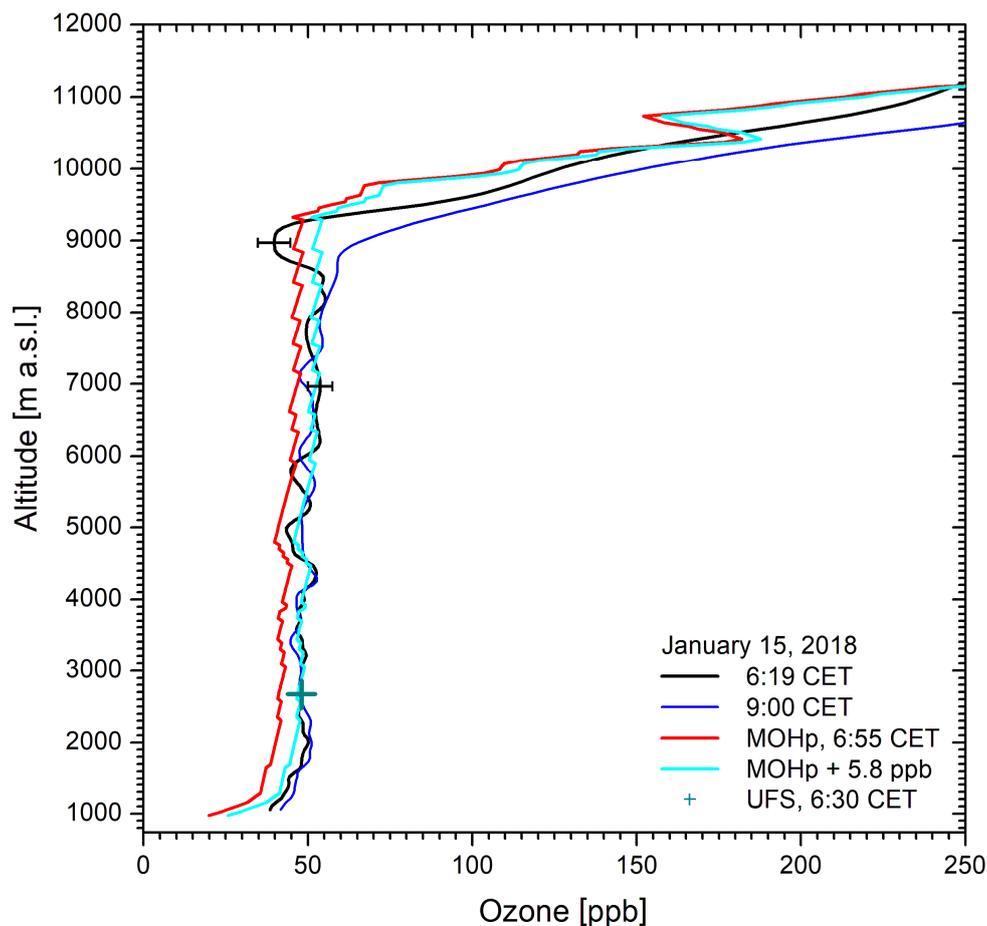
Fig. 4. Ozone measurements on 15 January 2018: The MOHp ozone (red) is also shown shifted by 5.8 ppb to match the lidar ozone (cyan), in part the black, in part the blue curve. Differences exist in the tropopause region, which is frequently the case. The sawtooth structure in the MOHp data is due to insufficient digital resolution in the NDACC data base.

835
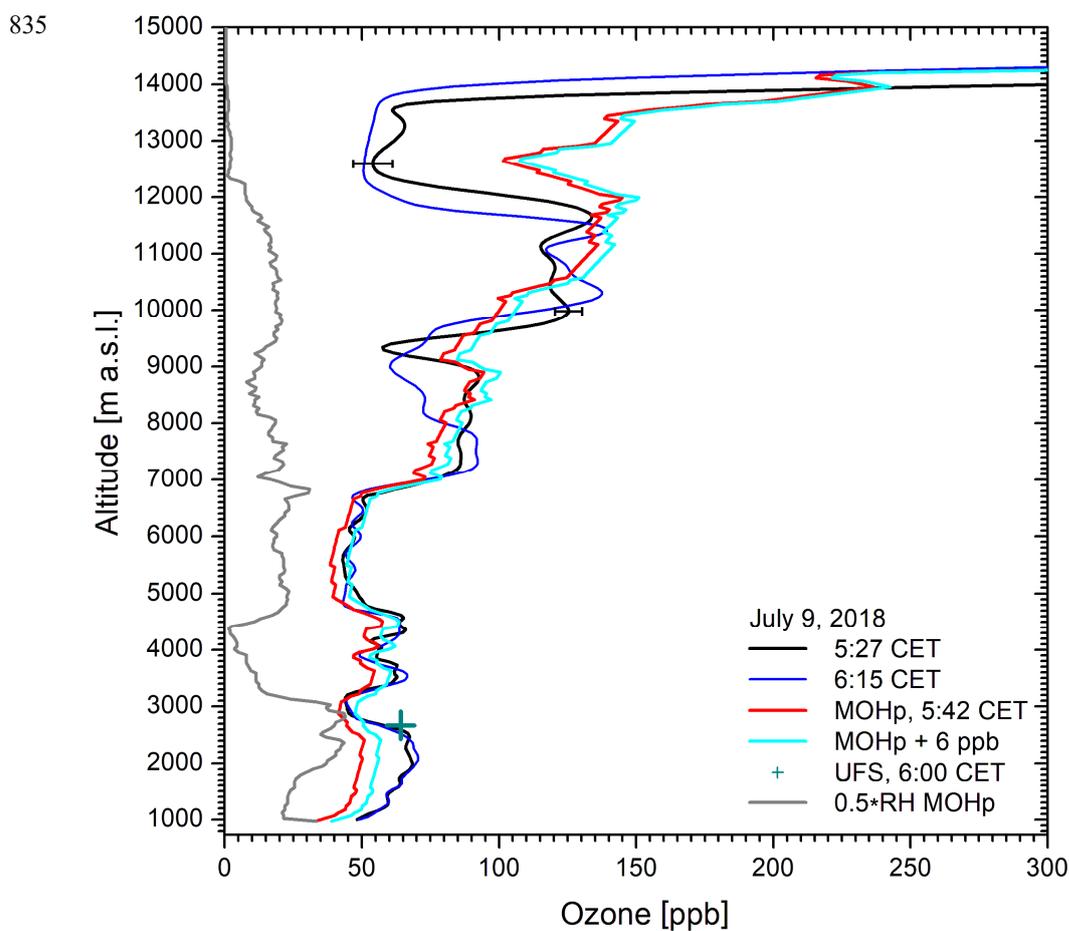
Fig. 5. Summertime ozone measurements (July 9, 2018) with pronounced layering; the sonde ozone (red) is brought to reasonable agreement with the lidar (black curve) above 2.7 km by adding 6 ppb (cyan). Above 9 km the air masses are no longer comparable. The particularly strong discrepancy of the UFS *in-situ* ozone can be explained by orographic lifting of the ozone edge at 2.7 km. The moderate RH (grey) in the free troposphere indicates that the very high ozone values could be due to a stratospheric air component.
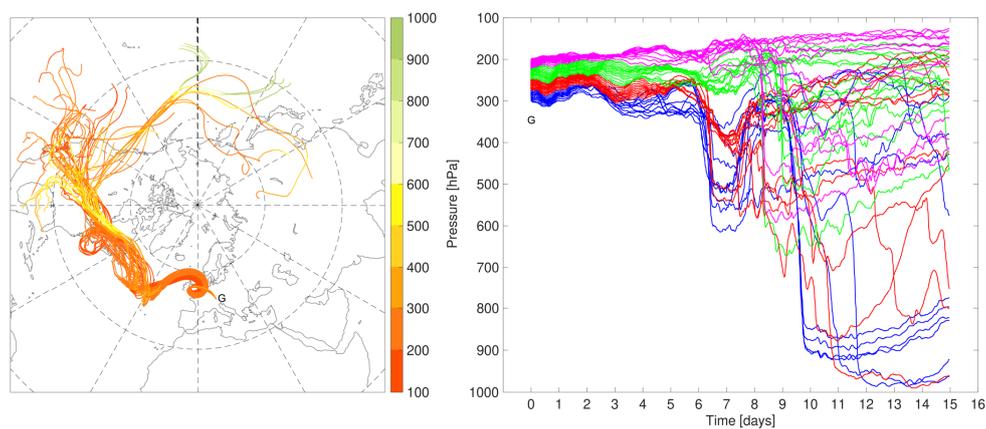
Fig. 6. 350-h LAGRANTO backward trajectories, started above Garmisch-Partenkirchen (G) on 9 July 2018 at 7:00 CET
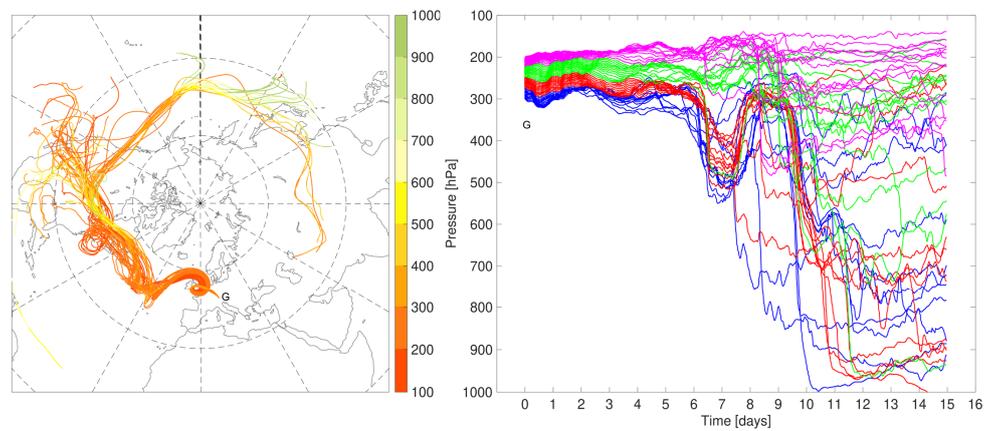
Fig. 7. 350-h LAGRANTO backward trajectories, started above Garmisch-Partenkirchen (G) on 9 July 2018 at 8:00 CET

847
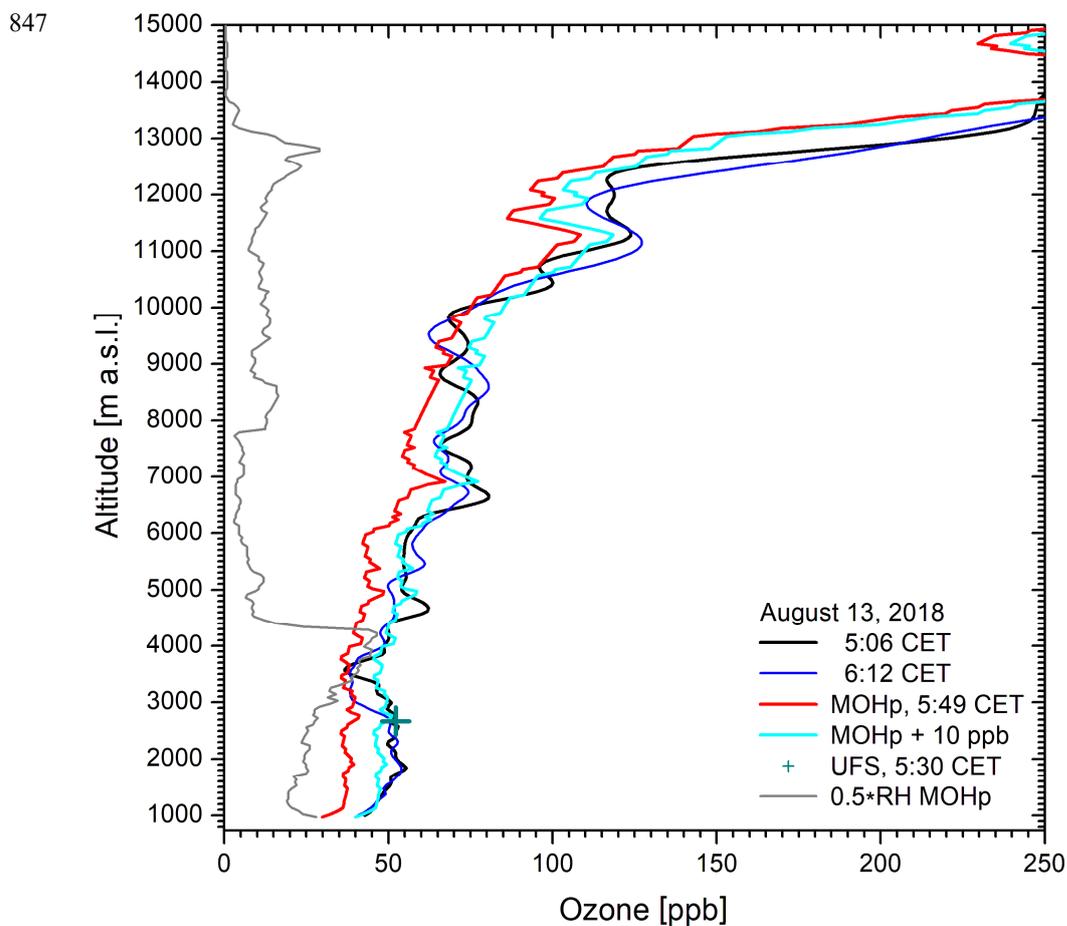
Fig. 8. Ozone measurements on 13 August 2018: The agreement of the shifted MOHp ozone profile (cyan) with
the lidar curves is rather good up to 12 km given the high summertime variability. The low to moderate RH
above 4.4 km (grey) indicates that the elevated ozone is partially caused by stratospheric air.

848
849
850
851

Atmospheric
Measurement
Techniques
Discussions
Open Access
EGU

852
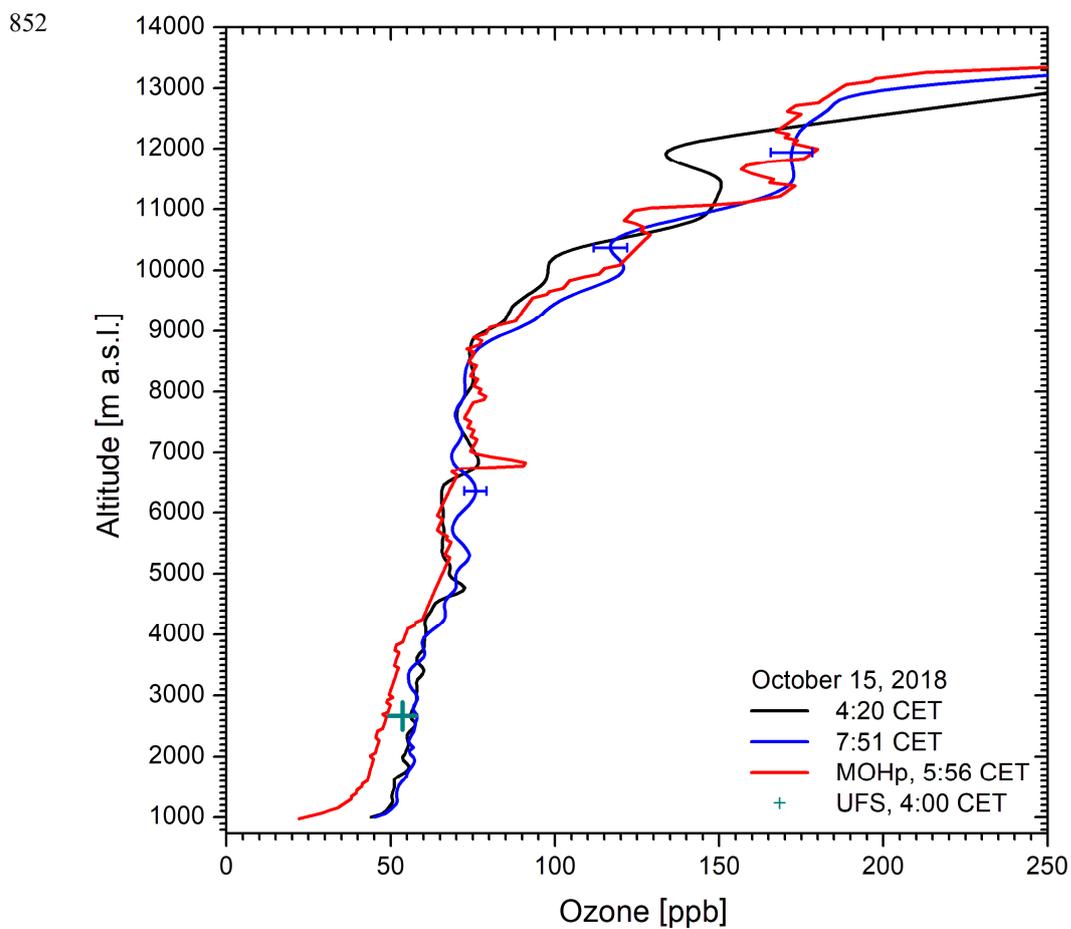
Fig. 9. Ozone measurements on 15 October 2018: The MOHp ozone (red) is not shifted. The agreement above 4.3 km is better with the earlier lidar measurement (black), above 7 km better with the blue curve. The lidar data are strongly smoothed in the stratosphere, as can be seen from the more detailed ozone structure in the sonde data. This example is one of the two examples with a pronounced low-altitude discrepancy between lidar and sonde extending to more the 3 km.

853
854
855
856
857
858

859
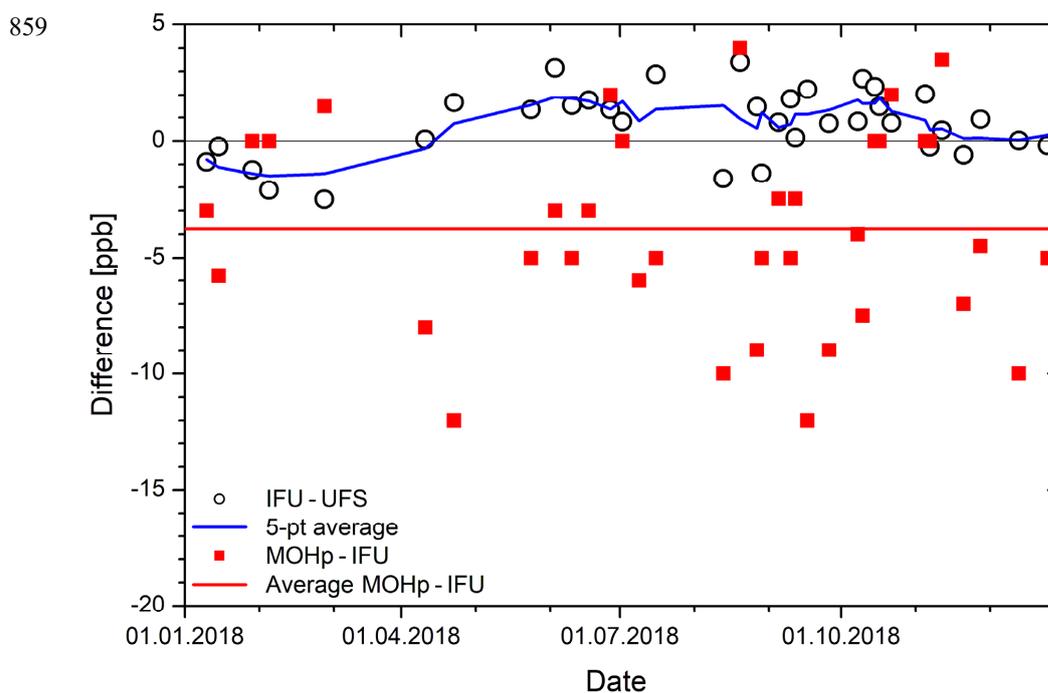
860 **Fig. 10**. Differences between the ozone values of the IFU DIAL at 2670 m and the UFS routine measurements as
861 well as the offsets of the MOHp profiles with respect to the DIAL for 35 of the 36 measurement days of the 2018
862 comparison. The blue curve represents a ±2-point running average of the differences between lidar and station.
863

Atmospheric
Measurement
Techniques
Discussions

Open Access

EGU

864
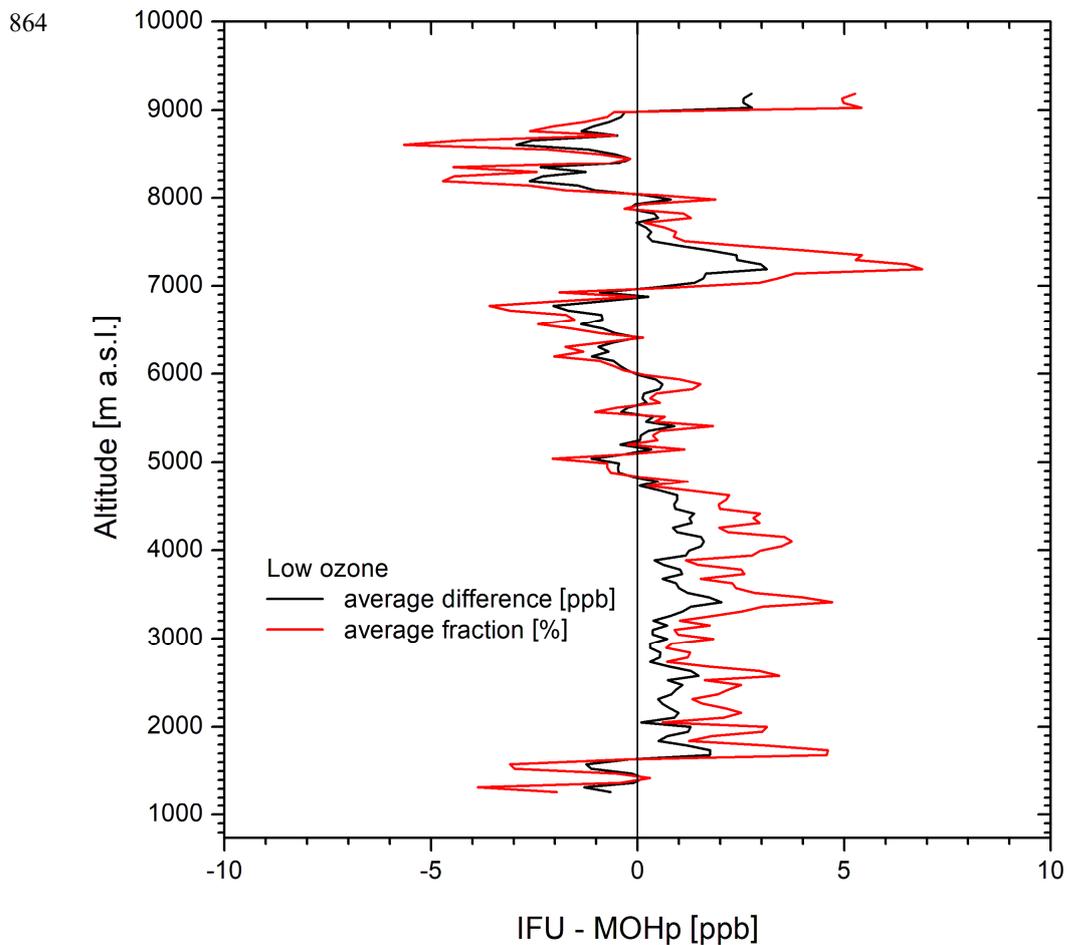
865 **Fig. 11.** Average differences between IFU lidar and offset-corrected MOHp sonde in 2018 for low-ozone
866 conditions (based on six cases); the uncertainties may be estimated from the maximum differences around these
867 altitudes.
868

869
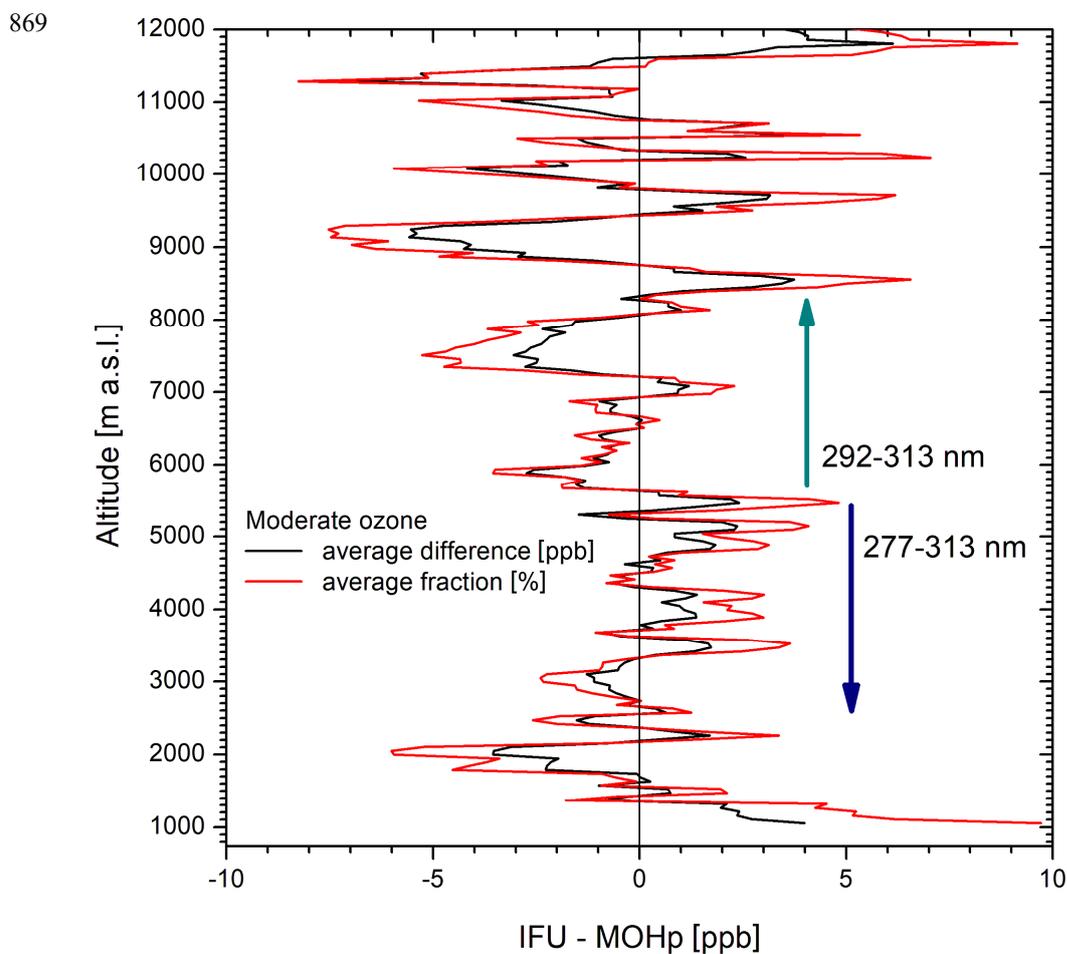
870 **Fig. 12.** Average differences between IFU lidar and offset-corrected MOHp sonde in 2018 for moderate-ozone
871 conditions (based on seven cases); we also indicate the altitude ranges of the two wavelength pairs used for the
872 lidar data evaluation.
873

Atmospheric
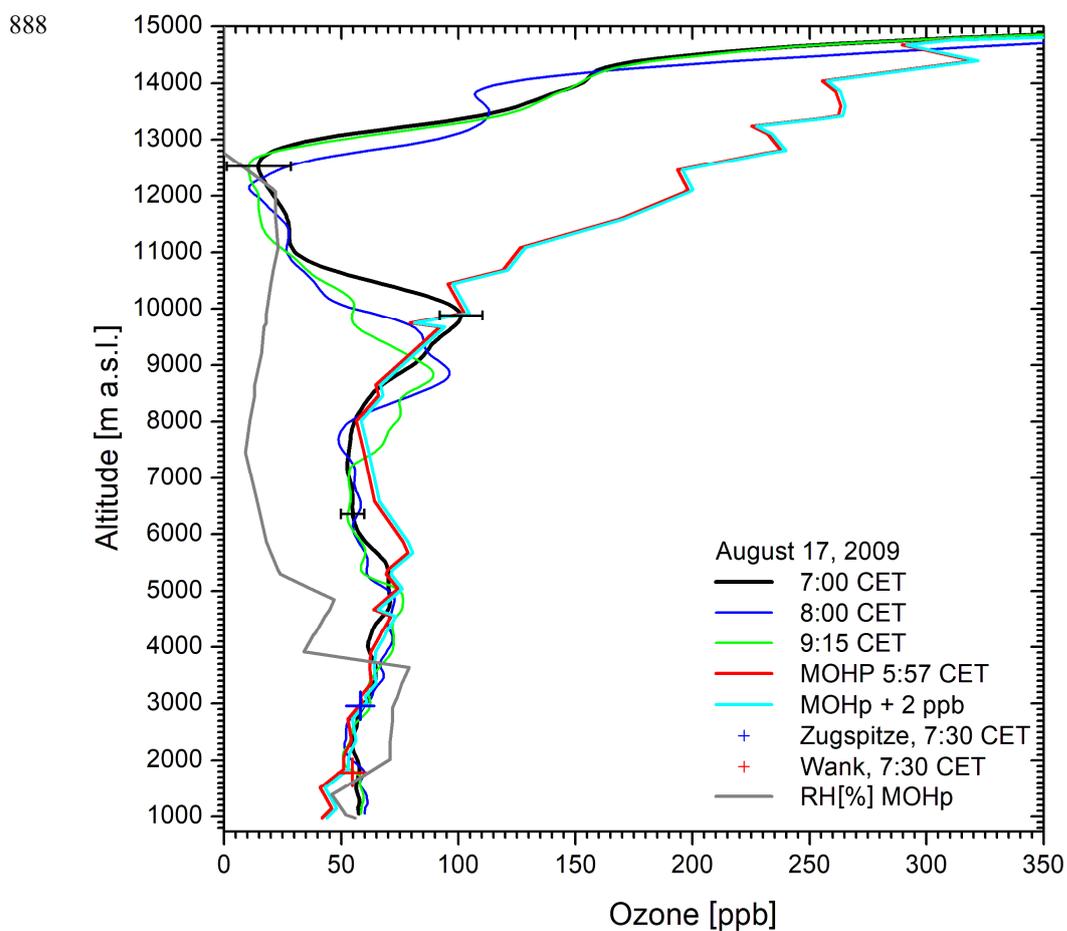Measurement
Techniques
Discussions

874
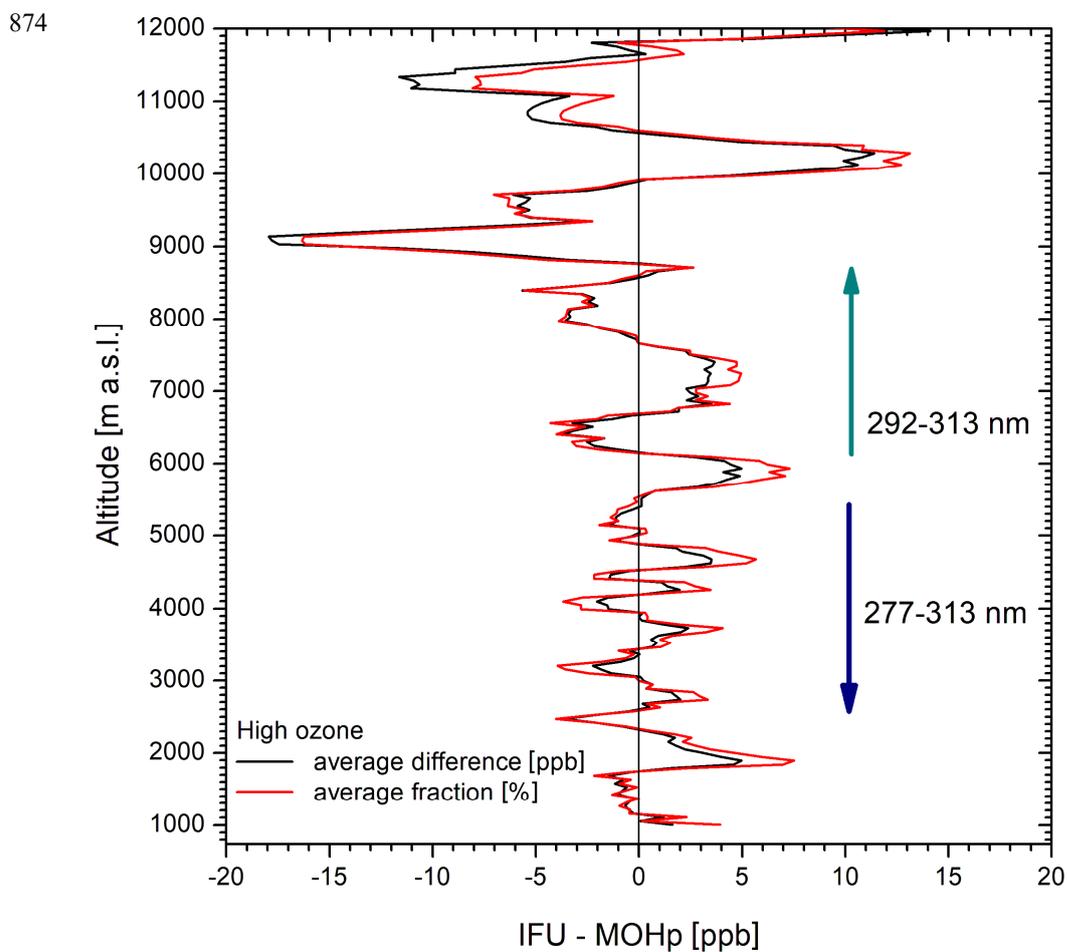
875 **Fig. 13.** Average differences between IFU lidar and offset-corrected MOHp sonde for high-ozone conditions
876 (based on six cases); we also indicate the altitude ranges of the two wavelength pairs used for the lidar data
877 evaluation.
878
879
880

881
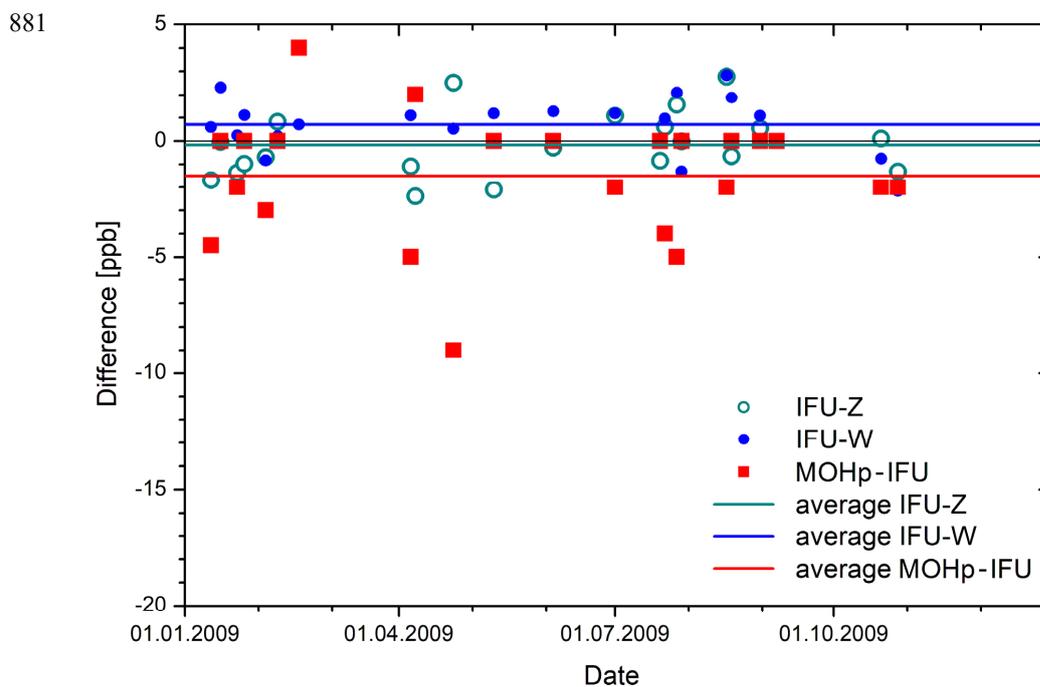
882 **Fig. 14**. Differences between the ozone mixing ratios of the lidar (IFU) and the stations Zugspitze (Z), Wank

883 (W) at the summit altitudes, and offsets between lidar and MOHp sonde

884

885
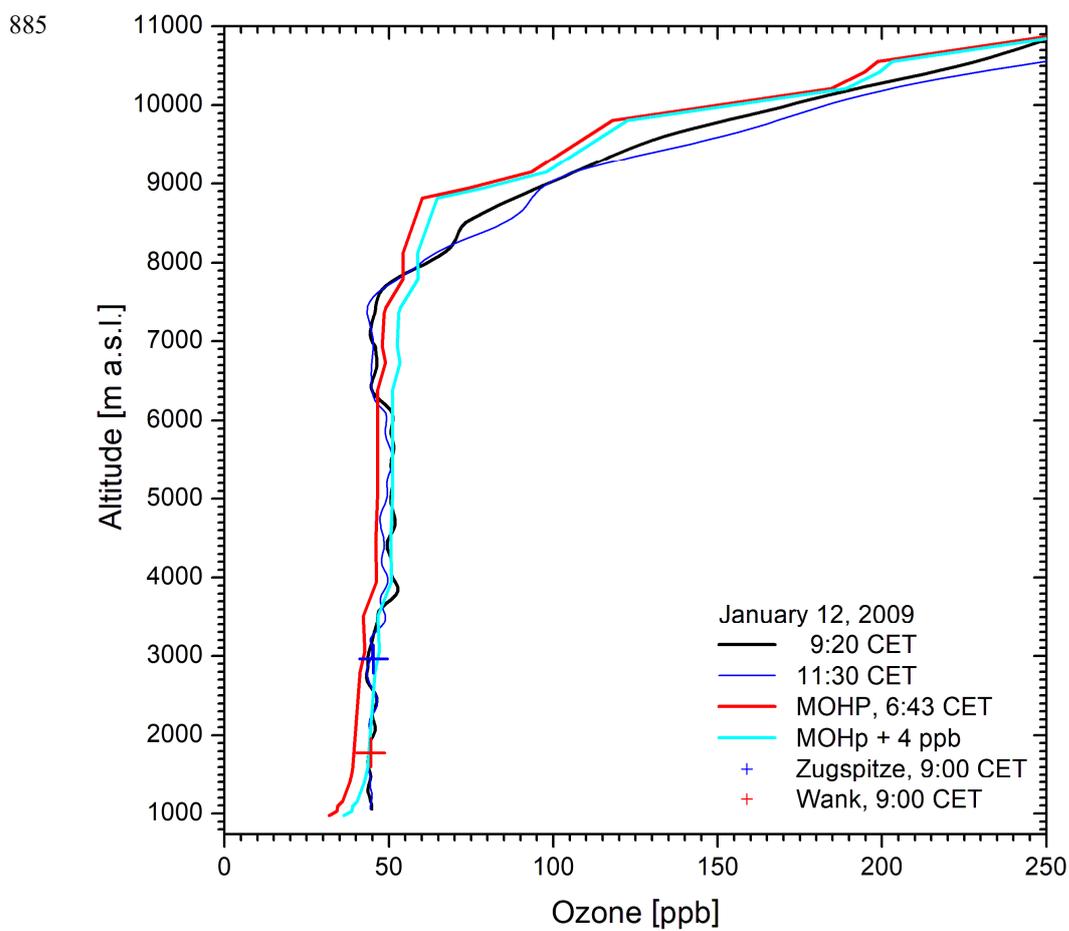
886 **Fig. 15**. Ozone measurements on 12 January 2009

887

888

Fig. 16. Ozone measurements on 17 August 2009; the structure in the upper troposphere is strongly influenced
by smoothing. The bias between 5.5 and 8 km has not been explained.

889

890

891

892
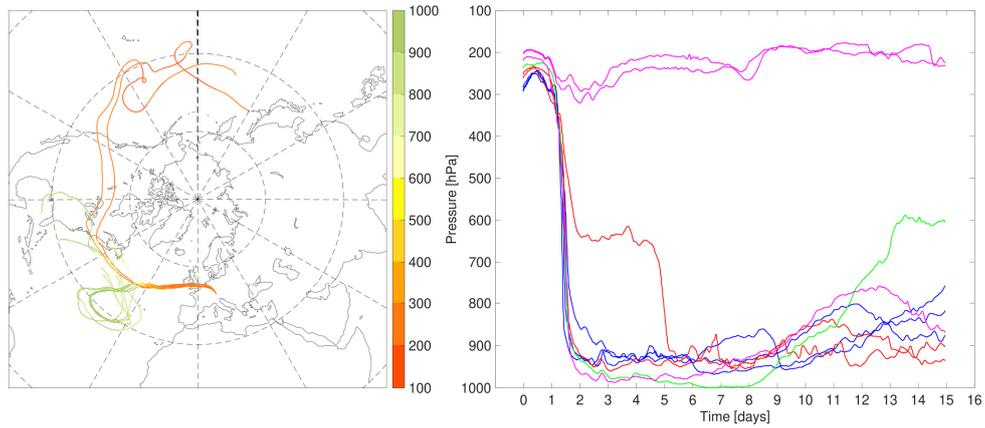
893 **Fig. 17.** 350-h LAGRANTO backward trajectories, started above Garmisch-Partenkirchen (G) on 9 July 2018 at
894 7:00 CET
895

896
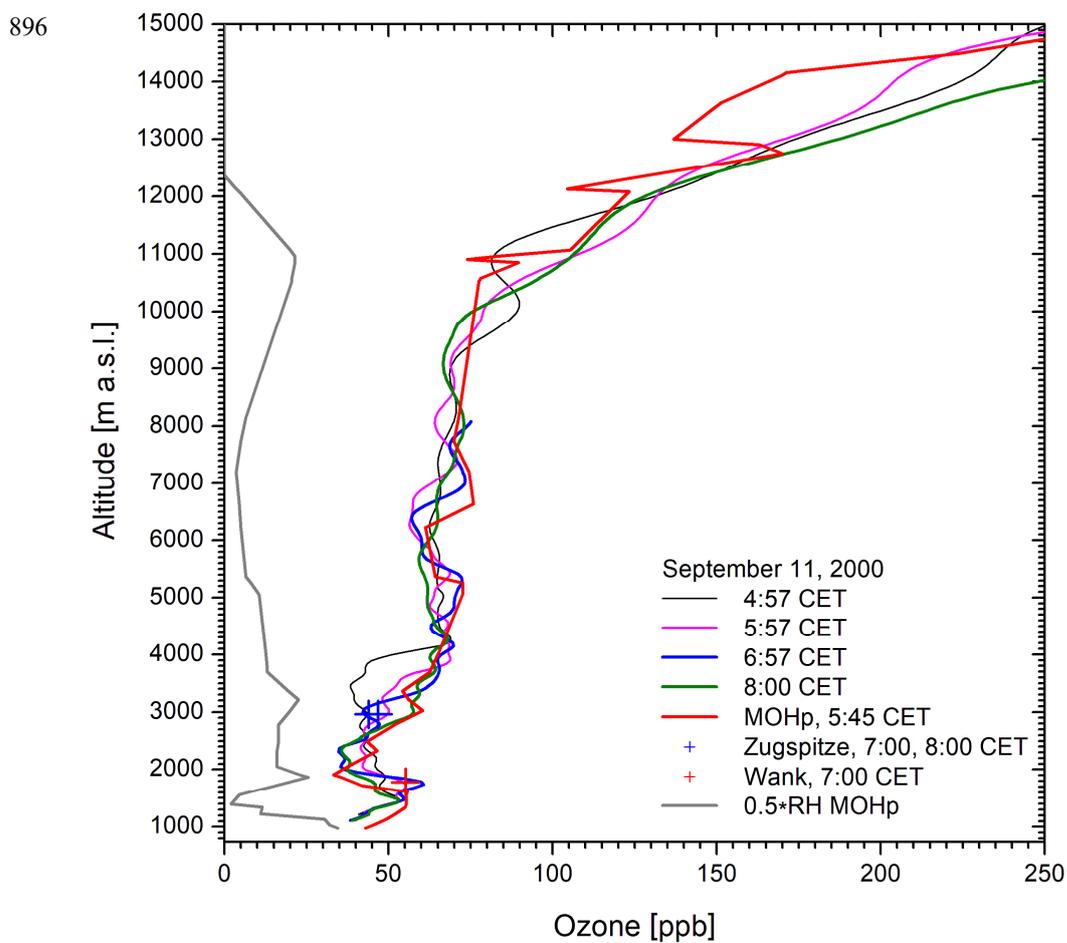
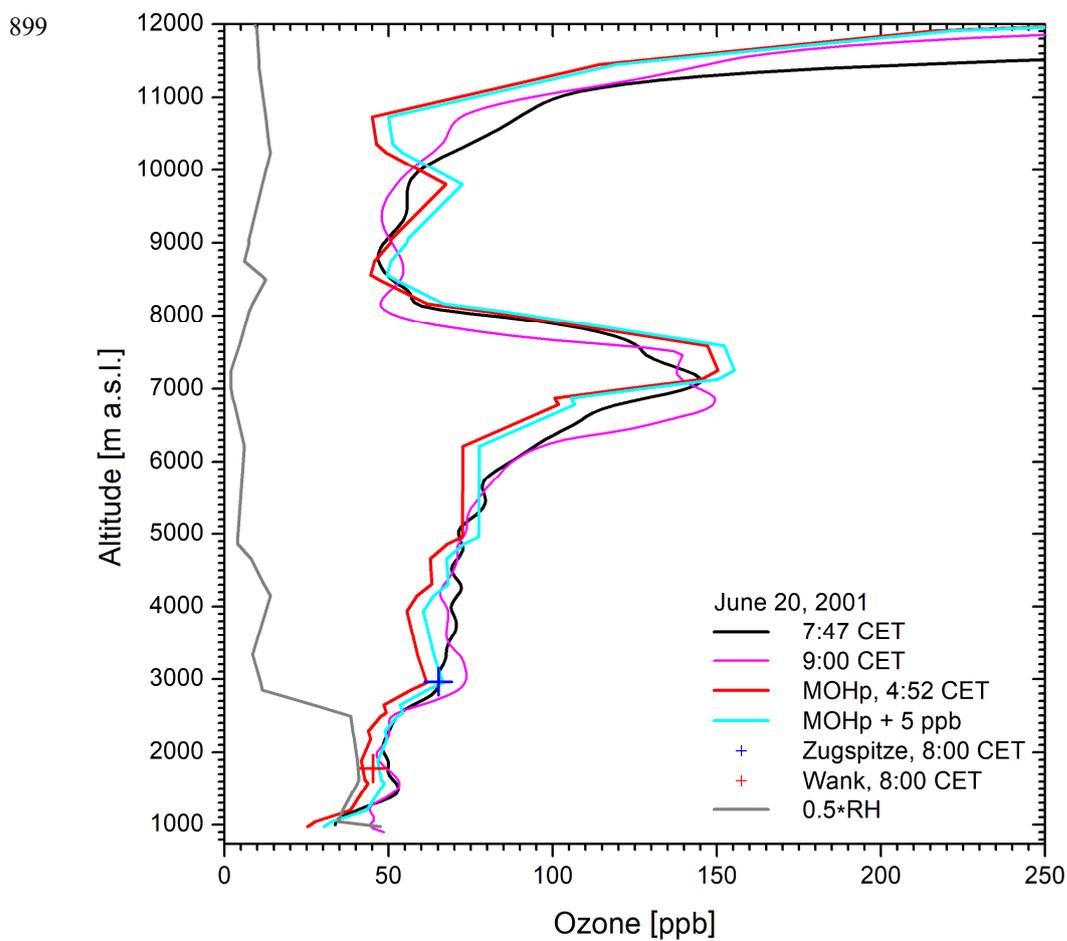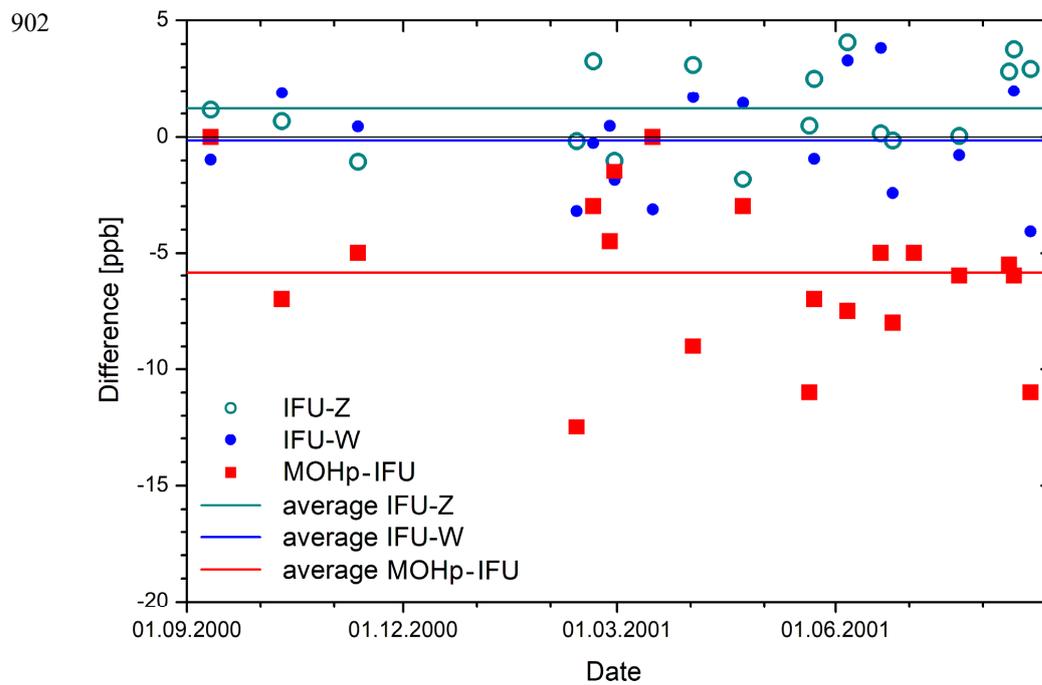897   **Fig. 18**. Ozone measurements on 11 September 2000

898

899

900   **Fig. 19**. Ozone measurements on 20 June, 2001

901

902

Fig. 20. Differences between the ozone mixing ratios of the lidar (IFU) and the stations Zugspitze (Z), Wank
(W) at the summit altitudes, and between lidar and MOHp sonde determined by shifting the sonde profile.

903

904

905

906

907